PATHOLOGICAL HETEROGENEITY IN MULTIPLE SCLEROSIS

A Thesis Submitted to the College of

Graduate Studies and Research

In Partial Fulfillment of the Requirements

For the Degree of Master of Science

In the Department of Anatomy and Cell Biology

University of Saskatchewan

Saskatoon

By

MYLYNE THAM

PERMISSION TO USE

In presenting this thesis/dissertation in partial fulfillment of the requirements for a Postgraduate degree from the University of Saskatchewan, I agree that the Libraries of this University may make it freely available for inspection. I further agree that permission for copying of this thesis/dissertation in any manner, in whole or in part, for scholarly purposes may be granted by the professor or professors who supervised my thesis/dissertation work or, in their absence, by the Head of the Department or the Dean of the College in which my thesis work was done. It is understood that any copying or publication or use of this thesis/dissertation or parts thereof for financial gain shall not be allowed without my written permission. It is also understood that due recognition shall be given to me and to the University of Saskatchewan in any scholarly use, which may be made of any material in my thesis/dissertation.

Requests for permission to copy or to make other use of material in this thesis in whole or in part should be addressed to:

Head of the Department of Anatomy and Cell Biology

University of Saskatchewan

107 Wiggins Road

Saskatoon, Saskatchewan, S7N 5E5

CANADA

ABSTRACT

Multiple sclerosis (MS) is an inflammatory, demyelinating disease of the central nervous system in which oligodendrocytes and myelin are targeted and destroyed by the body's immune system. Chemical elements such as iron, sulfur, and phosphorous are crucial in the synthesis and maintenance of myelin, and their imbalances have been linked to demyelination and neurodegeneration.

Early MS is heterogeneous with respect to its neuropathological features suggesting that the target of injury and the mechanisms of demyelination are different in different patient subgroups, also called immunopatterns. Using a multidisciplinary approach that combines synchrotron X-ray fluorescence imaging (XFI), histology and immunohistochemistry, I firstly investigated the heterogeneity of iron content and distribution in immunopattern II and III MS, to determine whether iron can be used as a marker to differentiate immunopatterns. XFI showed that iron was significantly increased in immunopattern II lesions ($p=0.003$) and predominantly stored as ferritin within myelin-laden macrophages. These observations prove that there is a profound iron heterogeneity in early active MS lesions and I propose that iron dysregulation plays an important role in the pathogenesis of MS lesions. My findings have potentially important clinical implications because iron may be used as a magnetic resonance imaging biomarker, allowing routine early immunopattern recognition in the clinical setting and advancing treatment approaches specific to the pathology.

The human brain is highly susceptible to oxidative damage due to its high concentrations of lipids and unsaturated fatty acids. Iron has been proposed to promote MS tissue injury through generation of toxic reactive oxygen species which damage carbohydrates, lipids, proteins, and DNA. Using XFI and Fourier-transform infrared imaging, I found that biopsied early MS lesions displayed increased oxidized lipids and aggregated proteins, and lower iron, sulfur, phosphorus and phosphate. The oxidative damage in early MS does is not driven by iron accumulation, and this argues against the use of iron chelators in the treatment of early MS.

Future studies will have to determine if the differential iron distribution between immunopatterns II and III MS is the result of different macrophage polarization in the two lesion patterns and/or is the expression of the iron's role in complement cleavage and activation characteristic of immunopattern II MS lesions.

ACKNOWLEDGEMENTS

I'd like to extend the most gratitude to my supervisor, Dr. Bogdan Popescu, for accepting me as a student and providing guidance and advice throughout the project. I'd like to thank my advisory committee: Dr. Jen Chlan and Dr. Ben Rosser for your valued feedback, and Dr. Dean Chapman for your generosity and support.

Thanks to the Department of Anatomy and Cell Biology, and Saskatchewan Innovation and Opportunity Scholarships for funding my work. Thank you to CIHR-THRUST for networking opportunities.

A huge thank you to Dr. Mark Hackett and Dr. Saroj Kumar for generously lending your expertise during data collection and analyses. Thank you to Drs. Sally Caine, Mariam Alaverdashvili for reading my drafts and providing excellent feedback. Thank you Dr. Dave Cooper for the teaching opportunities, Dr. Julia Boughner for providing well-needed wisdom, and Dr. David Schreyer for your advocacy and encouragement. Thank you to Anita Givens for expert lab technical support and many thanks to all my past and present colleagues at the CMSNRC for helping shape who I am today.

To my army of wonderful and fantastic friends that have stuck around this long: thank you for providing much needed wisdom, support, encouragement, forced exercise, and laughter to help me keep it together all these years. Isaac Pratt, I am truly grateful for your unwavering patience, encouragement, and understanding throughout the past three years – all fun times, right?

Finally, I am eternally grateful to my parents who have been encouraging throughout my academic journey and supportive in every way!

TABLE OF CONTENTS

PERMISSION TO USE i
ABSTRACT ii
ACKNOWLEDGEMENTS iii
TABLE OF CONTENTS iv
LIST OF TABLES vii
LIST OF FIGURES viii
LIST OF ABBREVIATIONS ix
Chapter 1 General Introduction 1
1.1 Multiple Sclerosis 1
1.2 Pathology of Multiple Sclerosis 2
1.2.1 Demyelination 4
1.2.2 Inflammation 7
1.2.3 Oxidative Injury 7
1.3 Elemental Distribution in MS 9
1.3.1 Iron Distribution 9
1.3.2 Sulphur Distribution 11
1.3.3 Phosphorous Distribution 12
1.4 Elemental Mapping Using Synchrotron Light 13
1.4.1 Synchrotron Radiation 13
1.4.2 X-ray Fluorescence Imaging 14
1.4.3 Fourier-transform Infrared Microspectroscopy 15
1.5 General Hypothesis and Research Objectives 16
1.5.1 General Hypothesis 16
1.5.2 Research Objectives 16
Chapter 2 Active Lesions in Immunopatterns II and III Multiple Sclerosis Display a Differential Iron Distribution 18
2.1 Introduction 18
2.1.1. Iron in MS lesions 18
2.1.2. Visualizing Iron in MS 19

2.1.3. Hypothesis 20
2.2 Materials and Methods 21
2.2.1 Sample Preparation 21
2.2.2 Histology and Immunohistochemistry 21
2.2.3. Characterization of Immunopatterns 22
2.2.4. X-ray Fluorescence Imaging 22
2.2.5 Chemically Specific Imaging 22
2.2.6 Image Analysis 24
2.2.7 Iron Quantification 24
2.2.8 Statistical Analysis 24
2.3 Results 24
2.3.1 Pathological Characteristics of Immunopatterns II and III 24
2.3.2 Immunopattern II Lesions Contained More Iron Than Immunopattern III Lesions and Iron Localized Within Macrophages 27
2.3.3 Ferric Iron is the Predominant Iron Species in Macrophages 30
2.3.4 H-Ferritin Localizes to Nuclei of Oligodendrocytes in PPWM of Immunopattern III Lesions 30
2.4 Discussion 33
Chapter 3 Oxidative Injury in Active Multiple Sclerosis Lesions 37
3.1 Introduction 37
3.1.1 Oxidative Injury and MS 37
3.1.2. Aim of Study 40
3.2 Materials and Methods 40
3.2.1 Sample Preparation 40
3.2.2 Histology and Immunohistochemistry 40
3.2.3 X-ray Fluorescence Imaging 41
3.2.4 Chemically Selective Imaging 41
3.2.5 Fourier-transform Infrared Microspectroscopy 41
3.2.6 Image Analysis 42
3.2.7 Statistical Analysis 42
3.3 Results 42

3.3.1 Tissue Pathology 42
3.3.2 Differential Distribution of Sulphur, Phosphate, And Iron in Demyelinated Lesions and Periplaque White Matter 43
3.3.3 Ferrihydrite is the Predominant Iron Species in Perivascular Macrophages 45
3.3.4 Lipid Oxidation Precedes Oxidation of Proteins 47
3.4 Discussion 53
Chapter 4 General Conclusions and Future Directions 57
Chapter 5 References 59

LIST OF TABLES

Table 2.1 Primary antibodies used for immunohistochemistry..... 23

Table 3.1 Integrated intensities of molecular vibration bands of lipid, protein and phosphate. .. 51

LIST OF FIGURES

Figure 1.1 A characteristic infrared spectrum of a biological sample displaying major macromolecular functional groups. 17
Figure 2.1 Activation of complement on myelin and within macrophages and equal loss of myelin proteins are characteristic for immunopattern II MS lesions. 25
Figure 2.2 Preferential loss of myelin-associated glycoprotein and the preservation other myelin proteins is characteristic for immunopattern III MS lesions. 26
Figure 2.3 Immunopattern II lesions contain more iron than immunopattern III lesions and iron localizes to macrophages. 28
Figure 2.4 Statistical analysis of iron in active lesions show more iron in immunopattern II lesions. 29
Figure 2.5 Ferrihydrite of ferritin is the predominant iron species in all samples and is highest in immunopattern II lesions. 31
Figure 2.6 Ferritin heavy chain (H-ferritin) localizes to oligodendrocyte nuclei in immunopattern III PPWM, and to the cytoplasm of oligodendrocytes in immunopattern II PPWM. 32
Figure 3.1 X-ray fluorescence imaging of an MS biopsy reveals loss of sulphur and phosphorous in demyelinated lesions, and accumulation of phosphorous and iron in perivascular macrophages. 44
Figure 3.2 Chemically specific XFI shows most iron in demyelinated lesions and normal appearing white matter is stored as ferrihydrite. 46
Figure 3.3 Infrared imaging of demyelinated lesion of an MS biopsy shows oxidation of proteins and lipids. 49
Figure 3.4 FTIR analysis shows increase lipid oxidation, accumulation of beta sheets and loss of phosphate in demyelinated lesions. 50
Figure 3.5 Graphical summary of oxidative damage markers in MS lesions compared to PPWM. 52

LIST OF ABBREVIATIONS

4-HNE	4-hydroxynonenal
ADEM	acute disseminated encephalomyelitis
ADP	adenosine diphosphate
AQP4	aquaporin-4
ATP	adenosine triphosphate
BBB	blood-brain barrier
BL	beam line
CH_2	methylene group
CH_3	methyl group
CIS	clinically isolated syndrome
CLS	Canadian Light Source
cm	centimetre
cm^{-1}	wavenumber
CNS	central nervous system
C=O	carbonyl group
COX	cyclooxygenase
CSF	cerebrospinal fluid
^{o}	degrees
^{o}C	degrees Celsius
DAB	3,3’-diaminobenzidine

DNA	deoxyribonucleic acid
eV	electron volt
Fe	iron
Fe^{2+}	ferrous iron
Fe^{3+}	ferric iron
Fe-S	iron-sulfur
FPA	focal plane array
FTIR	Fourier-transform infrared
GEE	generalized estimating equation
GRE	gradient recalled echo
HCl	hydrochloric acid
HE	hematoxylin – eosin
I0	ion chamber prior to sample stage
IgG	immunoglobulin G
IP	immunopattern
IR	infrared
INF-γ	interferon gamma
iNOS	inducible nitric oxide
KB	Kirkpatrick-Baetz
keV	kilo electron volt
LFB	Luxol-fast blue

MAC	membrane attack complex
MAG	myelin-associated glycoprotein
µm	micron
mM	millimolar
MHC	major histocompatibility complex
MOG	myelin oligodendrocyte glycoprotein
MBP	myelin basic protein
MRI	magnetic resonance imaging
MS	multiple sclerosis
ms	millisecond
NADPH	nicotinamide adenine dinucleotide phosphate
NMO	neuromyelitis optica
NO	nitric oxide
NOX	nicotinamide adenine dinucleotide phosphate oxidase
NOX1	nicotinamide adenine dinucleotide phosphate oxidase 1
NOX2	nicotinamide adenine dinucleotide phosphate oxidase 2
OPCs	oligodendrocyte precursor cells
%	percent
PLP	proteolipid protein
PPWM	periplaque white matter
SDs	standard deviations

SMAK	Sam’s Microtoolkit
SSRL	Stanford synchrotron radiation lightsource
SWI	susceptibility weighted imaging
ROS	reactive oxygen species
RRMS	relapsing-remitting multiple sclerosis
TNF-α	tumour necrosis factor alpha
XFI	X-ray fluorescence imaging

Chapter 1 General Introduction

1.1 Multiple Sclerosis

An estimated 100,000 Canadians are living with multiple sclerosis (MS), which is a disabling disease with mean onset age in early adulthood and a female-male ratio of approximately 3:1 (Bove & Chitnis, 2014; Ransohoff, Hafler, & Lucchinetti, 2015). A population-based prospective study of Saskatoon, Saskatchewan MS patients found that about 27% of the patients were born in the city of Saskatoon, indicating a high local prevalence (Hader & Yee, 2007). MS prevalence varies worldwide with countries like Canada, which have large populations originating from Northern Europe, having more than 100-200 cases per 100,000 people (Milo & Kahana, 2010). This prevalence variability may be relevant to the etiology and pathology of MS. MS is an inflammatory, demyelinating disease of the central nervous system (CNS) with a poorly defined and complex pathogenesis (Ingram, Hakobyan, Robertson, & Morgan, 2009).

Much progress has been made in MS research over the years; however, there is no prevention or cure, and treatment responses remain largely unpredictable. By describing MS as a disease with demyelinating lesions in the CNS, a wide variety of disorders can become compiled under one umbrella term. By that description, past research sought a single cause of MS and thus, a single therapy that would work for all MS patients. However, this focus does not take into account the clinical, genetic, and radiographic heterogeneity that affects the variability of patient responses to any given therapy (Popescu & Lucchinetti, 2012b). Currently, researchers are moving away from the single therapy approach because there is a large body of evidence strongly suggesting that MS results from complex interactions between genetics and environmental factors (Milo & Kahana, 2010).

A longitudinal study reported that multiple active lesions within the same individual have the same pattern (Lucchinetti et al., 2000). The authors studied tissues serially collected at either two different biopsies or at biopsy and then at autopsy, and found that the pattern of lesions from the same patient remained consistent over the time points. They also showed that other active lesions at different sites exhibited the same pattern within the same patient (Metz et al., 2014). This suggests that the targets of injury and mechanisms of demyelination in early MS might be fundamentally different in MS patient subgroups (Bitsch & Bruck, 2002; Lucchinetti et al., 2000).

1.2 Pathology of Multiple Sclerosis

Although no target antigen has been identified as proof for MS as an autoimmune disease, it is generally believed that tissue damage is driven by an "inflammatory process of a putative autoimmune nature" (Lassmann, Bruck, & Lucchinetti, 2007). The neuropathological hallmark of MS is a demyelinated lesion encompassing various levels of inflammation, gliosis, demyelination, and axonal damage (Filippi et al., 2012). Lesions form in the grey matter (Popescu & Lucchinetti, 2012a) and white matter of the brain (Lassmann, 2014a).

In the brain, the gray matter forms the outer covering called cortex and also forms clusters deep within the white matter of the forebrain and cerebellum called nuclei. Gray matter contains cell bodies, dendrites, and axons of neurons, as well as glial cells (Martini, Timmons, & Tallitsch, 2015). Cortical lesions and atrophy are thought to be the earliest pathological event in the MS disease course and in some MS cases, preceding the formation of white matter lesions (Calabrese & Gallo, 2009; Popescu & Lucchinetti, 2012a). Neuronal loss and apoptosis, loss of dendrites, and transected axons have been reported in cortical MS lesions (Peterson, Bo, Mork, Chang, & Trapp, 2001; Wegner, Esiri, Chance, Palace, & Matthews, 2006). Neurons are important functional units of the nervous system and consist of a cell body containing a large, round nucleus and a distinctive nucleolus. Dendrites extend from the cell body and receive information from other neurons, while axons transmit impulses away from the cell body to the synaptic terminals where the neuron communicates with another neuron or an effector organ (Martini et al., 2015; Ross & Pawlina, 2011). Damage to these structures impairs information processing in the cortex and may contribute to cognitive defects observed in MS patients (Popescu & Lucchinetti, 2012a).

White matter in the brain contains only myelinated neuronal axons and their associated glial cells and blood vessels (Blumenfeld, 2010; Gartner & Hiatt, 2007; Ross & Pawlina, 2011). Glial cells in the CNS include microglia, astrocytes, ependymal cells, and oligodendrocytes. Normally, microglia are immunocompetent cells that are constantly scanning the microenvironment for foreign invaders and are the first line of defense against tissue injury or pathogens. They are known as the "CNS professional macrophages" and serve as housekeepers of the microenvironment, cleaning up accumulated metabolic products and cellular debris (Farina, Aloisi, & Meinl, 2007; Katsumoto, Lu, Miranda, & Ransohoff, 2014; Mildner et al., 2007; Prinz & Mildner, 2011). Their various functions include phagocytosis and antigen presentation; but

under intense acute activation or chronic activation, microglia become neurotoxic (London, Cohen, & Schwartz, 2013). They produce cytokines, complement components, excitatory neurotransmitters (glutamate), and free radicals (Cross & Piccio, 2014; London et al., 2013) that can participate in the evolution of MS lesions.

Astrocytes are star-shaped glia and are the most abundant cells in the CNS. They provide physical and metabolic support for neurons and help maintain the tight junctions of the capillaries that form the blood-brain barrier (BBB) (Gartner & Hiatt, 2007). Astrocytes have been implicated as modulators of myelination through secretion of factors that affect oligodendrocyte differentiation (S. C. Barnett & Linington, 2013). Current research also suggests that activated astrocytes may have neuroprotective roles via the innate immune system in lesioned areas. Reactive astrocytes outline the area of damage and control leukocyte migration across the BBB, repair the BBB, and support neuron survival, after a CNS insult (Farina et al., 2007).

Ependymal cells are cuboidal to columnar in shape and are organized in a single epithelial-like layer lining the ventricles of the brain and the central canal of the spinal cord. These cells have processes that extend into the brain parenchyma and directly communicate with other glial cells. Ependymal cells may be involved in monitoring the composition and circulation of cerebrospinal fluid (CSF). Modified ependymal cells join with the pia mater to form the choroid plexus, which is responsible for producing CSF (Gartner & Hiatt, 2007; Martini et al., 2015). Analysis of CSF for the presence of immunoglobulin G (IgG) oligoclonal bands, which are immunoglobulins specific to CSF, may be used as support towards a diagnosis of MS (Link & Huang, 2006). However, CSF is not commonly used anymore and is no longer a part of the diagnostic criteria for relapsing-remitting MS (Polman et al., 2011).

Oligodendrocytes are the glial cells in the CNS that produce and maintain myelin that encases axons. Myelin is integral for transmission of messages along the axon. Myelin is 70-80% lipid, and also contains protein and water. The major lipid components are cholesterol, phospholipids, and glycosphingolipids (Mancall & Brock, 2011). In MS, myelin and oligodendrocytes are targeted and destroyed by the body's immune cells resulting in large confluent demyelinated lesions.

1.2.1 Demyelination

Demyelinated MS lesions contain numerous macrophages. These may be monocyte-derived macrophages recruited from the circulation to help in place of microglia that have become neurotoxic and can no longer carry out protective functions in the damaged tissue (London et al., 2013). Early studies showed that macrophages were heterogeneous and could be used to differentiate demyelinating activity (Bruck et al., 1996). One diagnostic approach in pathologically classifying MS lesions is based on the presence and distribution of myelin-laden macrophages within the lesion (Popescu & Lucchinetti, 2012b). Lesions can be classified into five types: active, chronic active, smoldering demyelinated, inactive, or remyelinated (Popescu & Lucchinetti, 2012b).

1.2.1.1 Types of Demyelinated Lesions

Active lesions are demyelinated lesions infiltrated by macrophages containing cytoplasmic myelin debris. Reactive astrocytes and inflammatory infiltrates comprised mainly of T lymphocytes, some B lymphocytes, plasma cells, and granulocytes, are also present in these lesions. Oligodendrocytes are variably lost and there is some axonal injury indicated by axonal swellings and buildup of β-amyloid precursor protein. There is also extensive BBB damage that may lead to the invasion of the CNS by inflammatory cells (Popescu, Pirko, & Lucchinetti, 2013). Gadolinium enhancement on MRI shows BBB damage and suggests the presence of inflammation (Haacke et al., 2009).

Chronic active lesions are present more often in the progressive phases of MS. Macrophages accumulate at the lesion edge with few at the inactive centre and these lesions show astrogliosis and significant loss of oligodendrocyte axons. Inflammatory infiltrates are typically located perivascularly with an either an intact BBB or the BBB damage is too minimal to be detected by gadolinium enhancement (Popescu et al., 2013).

Smouldering lesions, also known as slowly expanding lesions, are typically seen only in the progressive phase. These are demyelinated lesions with a distinct rim of macrophages and microglia, but only a few contain myelin debris.

Inactive lesions are completely demyelinated and have either an absence of macrophages or few macrophages that do not contain myelin debris, a few microglia and a glial scar.

Inflammatory cells consisting of macrophages and microglia, lymphocytes, and plasma cells are also present.

Remyelinated lesions are sharply demarcated and have thinly myelinated axons and oligodendrocyte precursor cells (OPCs). The presence of the latter as well as the balance between pro- and anti-inflammatory environments determine the extent of remyelination (Patrikios et al., 2006; Popescu et al., 2013). Early stage remyelination is extensive, contains a lot of newly formed myelin sheaths and OPCs, and is often seen in active lesions of the early phase of MS. Shadow lesions are sharply demarcated and completely remyelinated lesions typical of late stage remyelination. Some shadow lesions contain nearly normal myelin thickness that is hard to differentiate from normal white matter (Popescu et al., 2013). Shadow lesions also show decreased axonal density, few inflammatory infiltrates surrounding blood vessels but do not contain myelin-laden macrophages (Patrikios et al., 2006).

1.2.1.2 Patterns of Demyelination

On the basis of the specific myelin degradation proteins present within macrophages, active lesions can be classified into early or late stages of demyelination. Macrophages containing minor myelin degradation products, such as myelin-associated glycoprotein (MAG) and myelin oligodendrocyte glycoprotein (MOG), indicate an early active lesion. Macrophages containing major myelin proteins, such as proteolipid protein (PLP) or myelin basic protein (MBP), are digested more slowly and indicate a late active lesion (Popescu et al., 2013). By identifying the stage of demyelination, early active white matter lesions can further be segregated into patterns of demyelination. A detailed and systematic neuropathological study performed on a large collection of early active MS lesions from biopsy and autopsy material found a significant heterogeneity of lesions and identified four patterns of demyelination with possible distinct disease mechanisms (Bitsch & Bruck, 2002; Lucchinetti et al., 2000). Only early active lesions were classified into patterns based on specific myelin protein loss; lesion characteristics and location; oligodendrocyte destruction; and immunoglobulin (Ig) deposition and complement activation (Lucchinetti et al., 2000). Early active lesions are required for pattern classification because it implies that the disease is active and they also represent early stages of lesion development (Metz et al., 2014).

Demyelination in immunopatterns I and II is primarily immune-mediated and is propelled by activated macrophages that destroy and phagocytose myelin. Demyelination in these two

patterns occurs on a background of inflammation. Immunopattern I occurs in approximately 15% of biopsied patients and is a T-cell/macrophage-mediated demyelination. Lesions are sharply demarcated, situated perivascularly and lack immunoglobulin deposition and complement activation.

Immunopattern II lesions are found in about 58% of biopsied patients and are also T cell/macrophage-mediated demyelination; however, the major feature found exclusively in immunopattern II is the prominent deposition of immunoglobulins and complement C9 neoantigen at sites of active myelin destruction and association with myelin degradation products within macrophages. This is suggestive of cellular and humoral mediated autoimmunity. Immunopatterns I and II frequently exhibit remyelinated lesions with loss of oligodendrocytes at actively demyelinating sites and appearance of OPCs in the inactive region (Lucchinetti et al., 2000; Popescu et al., 2013).

Immunopatterns III and IV lesions have been primarily associated with oligodendrogliopathy (Lucchinetti et al., 2000). Immunopattern III is found in 26% of biopsied patients and the lesions are not well defined with active demyelination and oligodendrocyte apoptosis. Oligodendrocyte loss extends into the normal-appearing white matter and there is an absence of oligodendrocytes at the inactive centre. Remyelinated lesions are not observed. A striking feature of immunopattern III demyelinated lesions is the preferential loss of MAG in comparison to other myelin proteins, such as PLP or MOG. MAG is located in the periaxonal layer of myelin on the distal processes of oligodendrocytes. The loss of MAG is associated with a “dying back oligodendrogliopathy”, and oligodendrocyte death by apoptosis. “Dying-back oligodendrogliosis” is indicative of metabolically stressed oligodendrocytes that are no longer able to support their distal processes (Lucchinetti et al., 2000; Popescu & Lucchinetti, 2012b). Interestingly, preferential loss of MAG has also been observed in acute white matter ischemia (Aboul-Enein et al., 2003). This suggests that hypoxia-like injury, potentially via mitochondrial dysfunction, may be involved in the pathogenesis of immunopattern III lesions (Mahad, Ziabreva, Lassmann, & Turnbull, 2008).

Immunopattern IV lesions are rare and are found in approximately 1% of autopsy tissues from patients with progressive MS. They feature significant non-apoptotic oligodendrocyte death in the white matter surrounding the active lesion. (Lucchinetti et al., 2000; Popescu & Lucchinetti,

2012b). It is possible that the oligodendrocytes have some genetic defect that makes them more susceptible to the effect of inflammatory processes (Lassmann, 2014a; Popescu et al., 2013).

1.2.2 Inflammation

Gadolinium enhancement in MRI can identify BBB damage that leads to infiltration of inflammatory cells into the CNS (Filippi et al., 2012; Popescu et al., 2013). Inflammatory infiltrates are present at every stage of the disease and may even be present without ongoing active demyelination (Lassmann, 2014b; Lucchinetti, 2011). However, it has been noted that anti-inflammatory, immunomodulatory or immunosuppressive therapies are relatively effective in the early disease phase, but appear less effective in the progressive phase. This suggests that inflammation may play a significant role in tissue injury in the early stage of disease, whereas, neurodegenerative processes may drive the progressive stage (Lassmann, 2014a; Lassmann et al., 2007).

The inflammatory infiltrates in MS demyelinating lesions are primarily composed of CD8-positive cytotoxic T lymphocytes, and phagocytic macrophages derived from either monocytes or microglia (Bruck et al., 1995; Mahad, Trapp, & Ransohoff, 2005). $CD8^+$ T lymphocytes specifically recognize only antigens on Major Histocompatibility Complex (MHC) class I molecules and secrete lymphokines and perforins resulting in pathogen lysis (Ross & Pawlina, 2011). MHC I antigens are highly expressed in MS lesions on inflammatory cells, neurons, and glia (Lassmann et al., 2007). Monocytes are blood mononuclear cells that travel from bone marrow to differentiate into phagocytic cells of the mononuclear phagocytic system (Ross & Pawlina, 2011). With inflammation, all of the microglia and monocyte-derived cells can become tissue macrophages and these cells are involved in the immune processes underlying demyelination, such as myelin degradation, antigen presentation, lipid peroxidation, and production of cytokines (Bruck et al., 1995; Katsumoto et al., 2014). Components of destroyed myelin are targeted by macrophages and after internalization, the progression of degradation of specific myelin proteins occurs at different rates (Popescu & Lucchinetti, 2012b).

1.2.3 Oxidative Injury

Oxidative stress is suggested to play a critical role in the early, active stage of MS with contributions to neurodegeneration at later stages (Carvalho, Lim, Nijland, Witte, & Van Horssen, 2014). Oxidized deoxyribonucleic acid (DNA) and oxidized lipids are present within MS active

lesions and mainly accumulate in oligodendrocytes and myelin, which is associated with continuing demyelination. Oligodendrocytes make a lot of adenosine triphosphate (ATP) in order to support myelin membranes and have been shown to be more susceptible to oxidative stress than astrocytes and microglia *in vitro* (Mahad et al., 2008; Todorich, Pasquini, Garcia, Paez, & Connor, 2009).

Two main sources are responsible for creating reactive oxygen species (ROS): mitochondrial dysfunction and activated microglia and macrophages through oxidative burst (Carvalho et al., 2014). ROS are small oxygen-derived molecules that are oxidizing agents or can be converted to oxygen radicals (Bedard & Krause, 2007). ROS-producing enzymes such as nicotinamide adenine dinucleotide phosphate (NADPH) oxidases (NOXs) and inducible nitric oxide (iNOS) are highly expressed in macrophages and microglia to kill pathogens through a process called oxidative burst (Bedard & Krause, 2007; Carvalho et al., 2014). Macrophages and microglia have been identified as a major source of ROS in initial MS lesions compared with control white matter, with increased expression of NADPH oxidase-I (Nox1) and Nox2. This suggests that initial oxidative damage is driven by the inflammation-induced oxidative burst in activated macrophages and microglia. Oxidative damage then results in mitochondrial respiratory chain dysfunction, further propagating oxidative injury and ROS production (Fischer et al., 2012).

There are extensive mitochondrial disturbances in active immunopattern III MS lesions that result in energy deficiency (Lassmann, 2014a). The mitochondrial respiratory chain has four complexes, I-IV, and ATP synthase. The final respiratory chain complex, complex IV or cytochrome c oxidase [COX], is where 90% of oxygen is consumed and where proton pumping for ATP synthesis occurs (Mahad et al., 2008). Levels of subunit-I of complex IV (COX-I) and subunit-IV (COX-IV) are reduced in pattern III early active and late active lesions. Thus, mitochondrial defects lead to impairment of activity, assembly, and stability of complex IV (Mahad et al., 2008).

Mitochondrial injury and resulting energy disruptions have been shown to be a major driving factor of MS tissue injury (Haider et al., 2011). Normally, mitochondria produce ROS for signalling functions as a by-product of cellular respiration. However, when ROS production exceeds the cellular antioxidant capability, they can become critical mediators of oxidative stress resulting in damage to important cellular components such as lipids, proteins and DNA in early

and chronic stages of MS (Carvalho et al., 2014; Haider et al., 2011; van Horssen et al., 2008; Witte, Mahad, Lassmann, & van Horssen, 2014).

1.3 Elemental Distribution in MS

1.3.1 Iron Distribution

Metals play an important role in the CNS and are vital to essential functions such as energy production, nerve transmission, and oxygen transport. Iron (Fe) is an essential trace metal that plays a crucial role in physiological brain metabolism, oxygen transport, myelin synthesis, neurotransmitter production, and oxidative stress (Ropele et al., 2011). Iron is needed for oxidative metabolism and the brain has a high rate of oxidative metabolism most likely associated with the oligodendrocyte maintaining a myelin sheath that is 100 times its weight (Connor & Menzies, 1996). Myelin production and maintenance in the CNS depend on oligodendrocytes, the cells that stain for iron more robustly than any other cell in the adult brain, under normal conditions (Todorich et al., 2009). Numerous enzymes involved in cholesterol and lipid synthesis, which are both vital components of myelin and ATP production, require iron as a cofactor (Todorich et al., 2009).

Biologically, iron can be divided into heme iron and nonheme iron according to chemical structure and metabolism. Heme is a prosthetic group involved in oxygen transport, electron transport and oxidation-reduction reactions. Nonheme iron exists in a ferrous (Fe^{2+}) or ferric (Fe^{3+}) oxidation state and ferric iron is predominant in human brain (Schenck, 2010). Most of the iron in the human brain is stored as nonheme iron in oligodendrocytes and myelin (Hametner et al., 2013). Iron is a “redox active” metal because it can redox cycle between its ferrous and ferric oxidation states to catalyze oxidation-reduction reactions (Meguro et al., 2007; Schenck, 2010). Nonheme iron is involved in the production of cytotoxic hydroxyl radicals (OH·) through the Fenton reaction and the Haber-Weiss reaction (Crichton, 2009). OH· are highly reactive and have the ability to oxidize lipids, proteins, carbohydrates, and DNA (van Horssen et al., 2008). It has also been suggested that iron is liberated from destruction of myelin and this results in amplification of oxidative injury in MS lesions (Haider, 2015; Hametner et al., 2013). Iron levels must be regulated to avoid iron toxicity stemming from excess iron or iron deficiency (Ye & Rouault, 2010). The cell keeps iron either in the iron-transport system as transferrin or in the iron-storage system as ferritin and hemosiderin (Meguro et al., 2007).

Transferrin is an important protein that carries iron into the brain across the BBB. Iron accumulation is important during early brain development and iron is released from transferrin by microglia and delivered to OPCs (Todorich et al., 2009). However, as oligodendrocytes develop, there is a down-regulation of transferrin receptors and mature oligodendrocytes do not express transferrin receptors, even in hypomyelination conditions, yet oligodendrocytes still acquire iron (Leitner & Connor, 2012; Todorich et al., 2009).

The major iron delivery system to mature oligodendrocytes was shown to be ferritin. (Todorich, Zhang, & Connor, 2011). Ferritin is a ubiquitous and highly conserved protein that plays a major role in iron homeostasis by sequestering and storing iron in a non-toxic, redox-inactive, and soluble form. It is capable of storing up to 4,500 iron atoms in the form of ferrihydrite. Mammalian ferritins have variable amounts of heavy (H) and light (L) -chain ferritins (Zecca, Youdim, Riederer, Connor, & Crichton, 2004). The H subunits confers ferroxidase activity that catalyzes the aerobic oxidation of Fe^{2+} to Fe^{3+} and the L subunits have no enzymatic activity but is responsible for transferring the Fe^{3+} to the iron core. Most of the iron in the human brain is ferritin-bound and the primary function of ferritin is the storage of iron. This keeps the iron in a safe form where Fe^{3+} is not freely available for conversion to the toxic ferrous form used in oxidative reactions (Asano et al., 2015; Friedman, Arosio, Finazzi, Koziorowski, & Galazka-Friedman, 2011; Meguro et al., 2007). H-ferritin is the main iron delivery system to oligodendrocytes because it prevents loss of cell viability after transferrin deprivation, and microglia were shown to provide iron to oligodendrocytes via H-ferritin (Todorich et al., 2011). Oligodendrocytes have the reported ability to upregulate ferritin expression and synthesis during hypoxia, leading to iron sequestration, which is thought to be a protective mechanism against oxidative injury (Qi & Dawson, 1994).

A study looking at transferrin and H-ferritin binding in the normal human brain found that there was a non-overlapping pattern of distribution of the two iron storage proteins, with transferrin found primarily in grey matter and ferritin in white matter. This non-overlapping pattern was also observed in MS lesions and it was concluded that the presence of transferrin indicated the presence of immature oligodendrocytes and ferritin was associated with mature oligodendrocytes (Hulet, Powers, & Connor, 1999).

Iron dyshomeostasis and pathological deposition of iron have been associated with numerous MS disease processes such as continuing demyelination, remyelination, axonal damage, and neurodegeneration (LeVine, Bilgen, & Lynch, 2013; Stephenson, Nathoo, Mahjoub, Dunn, & Yong, 2014), MRI and histopathological studies have suggested that iron levels may have an effect on pathological mechanisms underlying MS and could be used to study heterogeneity of MS lesions (Bagnato et al., 2011; Yao et al., 2015). A study reported that ferritin levels in the CSF of chronic progressive active MS patients were higher than normal, while the levels of transferrin and iron did not significantly increase. The authors suggested that an elevated ferritin level was a defense mechanism against inflammatory processes occurring in the CNS, such as increased cytokine levels (LeVine et al., 1999). A later study showed that H-ferritin expression in oligodendrocyte precursors increased in response to higher iron levels and the presence of cytokines did not affect this increase (Zhang et al., 2005). The authors also mentioned that oligodendrocytes were more susceptible to toxicity from certain cytokines, such as TNF-α and IFN-γ, after iron loading. It was suggested that increased mitochondrial iron levels from the iron loading resulted in mitochondrial dysfunction and subsequent vulnerability of oligodendrocytes to TNF-α, IFN-γ, and oxidative injury (Zhang et al., 2005).

A study probed the elemental makeup of serum from MS patients and found that serum iron levels could be used to differentiate between patients with clinically definite MS and healthy donors. Patients with clinically definite MS had lower serum iron and higher serum oxidative status than healthy donors (Ristori et al., 2011). Oligodendrocytes and myelin also store iron accumulated in the human brain with age; thus, their destruction in the MS disease process may release this iron that can amplify harmful oxidative processes (Lassmann, 2014b). However, it is also possible that iron deficiency, which has been implicated in restless legs syndrome, drives pathology in MS (Connor et al., 2011). The existence of abnormal iron deposits and their exact role in MS remains to be elucidated.

1.3.2 Sulphur Distribution

Sulphur may also play a role in the pathogenesis of MS lesions. Iron is imported into mitochondria where it is used to synthesize iron-sulphur (Fe-S) clusters and serves as a cofactor for cytochromes a, b, and c. Fe-S clusters are involved in cell functions such as respiration, catalysis, and redox reactions (Todorich et al., 2009; Ye & Rouault, 2010). Fe−S proteins have

prosthetic groups comprising two or more iron atoms bridged by sulphur ligands, which facilitate multiple functions such as redox activity and enzymatic function (Ye & Rouault, 2010). Dysfunction of Fe–S cluster protein formation results in mitochondrial iron overload and cytosolic iron depletion in mammalian cells (Rouault, 2012). Damage to Fe-S clusters releases iron, which can then participate in the Fenton reaction to create ROS (Slauch, 2011).

Sulphur-containing amino acids are more abundant in animal proteins and sulphur is an integral part of numerous enzymes and antioxidant molecules, such as glutathione (Mukwevho, Ferreira, & Ayeleso, 2014). Glutathione is highly sensitive to cellular redox changes and indicates cellular oxidative stress, which could lead to its use as a biomarker in MS (Carvalho et al., 2014). Cysteine and methionine residues are very sensitive to oxidation by almost all ROS (Berlett & Stadtman, 1997). Methionine and cysteine residues are also vulnerable to oxidation by peroxynitrite (Berlett & Stadtman, 1997). Peroxynitrite is formed in a reaction between nitric oxide and superoxide and once formed, it can convert tyrosine residues into nitrotyrosine (van Horssen et al., 2008). Nitrotyrosine has been found to localize within myelin-laden macrophages and reactive astrocytes in active MS lesions and is a marker of oxidative damage (van Horssen et al., 2008). Elemental sulphur is a component of sulfatides, which combines with cerebrosides to form galactolipids, which are abundant constituents of myelin (Stuber et al., 2014).

1.3.3 Phosphorous Distribution

Myelin is made of 70% lipid and the specific lipids include cholesterol, galactolipids, and phospholipids (Stuber et al., 2014). Phosphorous is also found in the helical strands of DNA in phosphomonoester and phosphodiester proteins; and in phosphocreatine and nucleoside phosphates like ATP and adenosine diphosphate (ADP), which are important for energy storage and transfer. A significant amount of phosphorous is found in phospholipids, accounting for approximately 80% of all phosphorous in white matter and 60% in gray matter. This means that phosphorous can be used as a marker of myelin distribution (Stuber et al., 2014).

A study designed to analyze the presence and location of oxidized DNA and lipids in MS showed that oxidized DNA was found in areas with significant microglial activation at the lesion edge, apoptotic oligodendrocytes, and astrocytes. They also found oxidized phospholipids in oligodendrocytes and myelin, and degenerating axons and neurons, in active MS lesions (Haider et al., 2011). Lipid peroxidation occurs when ROS are produced close to lipid-rich cell membranes

and the resulting reactive aldehyde species diffuse throughout the cell and covalently modifies DNA, lipids, and proteins (Fritz & Petersen, 2011).

1.4 Elemental Mapping Using Synchrotron Light

1.4.1 Synchrotron Radiation

Synchrotron radiation is electromagnetic radiation emitted by electrons moving at relativistic speeds following a curved trajectory (Kim, 2009). The source of electrons is a tungsten-oxide disk located in an electron gun. High voltage electricity passes through this disk and heats it to about 1000°C, which allows electrons to escape the surface. There is a powerful positive charge that repels the released electrons in to the linear accelerator. The linear accelerator contains a series of radio frequency cavities, which are special cavities that transfer energy to passing electrons. From the linear accelerator, electrons enter the booster ring for another energy increase and then they travel at approximately the speed of light. These electrons are then injected into straight sections of the storage ring. Bend magnets inside the storage ring change the direction of the circulating electrons so they emit synchrotron radiation. Special magnets called insertion devices move the electrons back and forth in order to create higher flux photons, or more intense light, for the beamline. This synchrotron radiation then travels through a photon port towards experimental beamlines.

Each beamline consists of an optics hutch, experimental hutch, and work station. In the optics hutch, light is focused and a monochromator is used to separate different wavelengths. Once the relevant wavelengths are selected, mirrors focus the beam on to the sample in the experimental hutch and a detector picks up the data and sends it to the work station to be analyzed (Canadian Light Source, 2012). A microfocused X-ray beam excites specific elements within a sample to release X-ray fluorescence and numerous chemical elements can be investigated simultaneously (Pushie, Pickering, Korbas, Hackett, & George, 2014).

Synchrotron radiation is over 1000 times brighter than conventional sources and it is polychromatic and tunable, which provides a wider variety of experimental conditions (Webb & Roach, 2014).

1.4.2 X-ray Fluorescence Imaging

X-ray fluorescence imaging (XFI) is a powerful technique used to look at elemental and chemical species distributions in biological tissues at various spatial resolutions (Pushie et al., 2014). Used as an imaging method, XFI shows multiple metals simultaneously, which is an advantage over "single-metal" histochemistry (Popescu et al., 2009). The use of rapid-scan XFI has significantly increased the area that can be mapped and decreased the amount of time required to do so because it is a continuous raster scan of the sample. This is ideal for generating a map of global element distribution in large samples or whole sections of the brain (Popescu & Nichol, 2011). XFI requires minimal sample preparation, no equipment purchase is necessary, and beam time can be inexpensive. Experimentally, advantages are high spatial resolution, a wide array of elements can be examined, and data can be quantified. This technique is non-destructive and thus, the same samples can be subsequently analysed using a different technique like histology.

Tissue sections are collected on plastic, metal-free coverslips. The incident energy of the beam is selected and fixed so that all desired elements with K-shell absorption edges below the incident energy will be excited. A common incident energy is 13 keV, which can image elements with atomic numbers between 15 (phosphorous) and 34 (selenium). When the incident X-ray beam hits the sample, k-shell electrons of absorber atoms are excited and ejected in to the continuum, leaving a hole that is unstable. An outer shell electron will fall in to fill the core hole and this movement generates a fluorescent photon of a specific energy. A detector placed near the sample collects the X-ray fluorescent photons. To see the distribution of the element of interest, the specific k-edge emission energy of the element of interest is windowed on and the emitted spectrum is analyzed. Because XFI is based on the physics of the atom, every atom of the element excited by the beam will emit a fluorescent photon, regardless of its chemical state, oxidation state, or bound state (Popescu & Nichol, 2011). This is an advantage over iron visualization using Prussian blue and Turnbull because these histological stains are not reliable in detecting heme iron and iron tightly bound to other compounds in tissues (Meguro et al., 2007; Stuber et al., 2014).

Since all chemical forms of an element are detected simultaneously, chemically selective imaging is one method that can be used to differentiate between chemical forms. To do this, multiple incident energies are selected carefully to detect various chemical forms and a fluorescent map is collected at each energy. This method of imaging uses the sensitivity of near-edge spectra

to chemical species, but requires a prior knowledge of the probable composition of the element in the brain (Pushie et al., 2014).

The distribution of elements in human MS active lesions of different patterns in tissues obtained post mortem or at biopsy, has yet to be studied using XFI. XFI can provide further detailed information to substantiate MRI and histological data about the subcellular regulation of elements within lesions and normal-appearing white matter (PPWM) in MS lesions.

1.4.3 Fourier-transform Infrared Microspectroscopy

Various regions of the CNS can be differentiated using Fourier-transform infrared (FTIR) microspectroscopy based on the presence or absence of myelin (Caine, Heraud, Tobin, McNaughton, & Bernard, 2012). Chemical changes that underlie the process of demyelination in MS active lesions are reflected in the infrared spectrum as variations in band shapes and intensities of particular macromolecular functional groups (Caine et al., 2012). The infrared (IR) region of the electromagnetic spectrum lies just beyond the visible spectrum in the longer wavelength and lower frequency region. Mid-IR spectroscopy looks at molecular vibrations of internal (intra-) molecular bonds or of bonds between (inter-) molecules. The mid-IR region, specifically, spans the wavelength and wavenumber range of 2.5 µm (4000 cm^{-1}) to 25 µm (400 cm^{-1}). The wavenumber, expressed in cm, is the reciprocal of the wavelength and is typically used to interpret mid-IR spectra (Chalmers, 2011).

Modern IR spectroscopy is performed with a Michelson interferometer that is faster and has better signal to noise than dispersive mid-IR spectrometers. A Michelson interferometer has a scanning mirror that produces constructive and destructive interference patterns as it changes position, resulting in an interferogram. Fourier transform is a mathematical tool that is required to transform the interferogram into an absorbance spectrum (Chalmers, 2011).

When molecules are interrogated, they will absorb mid-IR radiation occurring at a frequency corresponding to the molecular vibrations and exhibit a characteristic absorption band (Chalmers, 2011). All organic functional groups have specific FTIR absorption bands, and particularly strong absorptions for fatty acyl moieties (methyl and methylene groups), proteins (amides I and II), and phosphate groups (nucleic acids, protein), which all fall within the mid-IR range. The FTIR spectra account not only for the chemical nature of cell molecules, but also for

their conformations (Goormaghtigh, Ruysschaert, & Raussens, 2006; Navea, Tauler, Goormaghtigh, & de Juan, 2006; Oberg, Ruysschaert, & Goormaghtigh, 2004).

Only two previous studies have used FTIR to study MS samples and both relied on autopsy samples from MS patients in the chronic stage of the disease (Choo, Jackson, Halliday, & Mantsch, 1993; LeVine & Wetzel, 1998). Since FTIR can provide *in situ* chemical information, this technique is ideal for analysing biopsies because it provides more insight into the earliest chemical changes occurring in MS lesions.

1.5 General Hypothesis and Research Objectives

1.5.1 General Hypothesis

The distribution of elements and markers of oxidative damage can be used as biomarkers to distinguish between the two most common patterns of MS lesions.

1.5.2 Research Objectives

My first research objective was to determine whether iron levels in active lesions of the most common MS immunopatterns, II and III, were different in post-mortem human brain tissue. Then we analyzed the localization of iron within the lesions and looked at the type of iron species present. To carry out this objective, I:

a) Used histopathology to classify and immunopattern active lesions and differentiate active lesions from PPWM.
b) Used XFI to localize iron and quantify levels of iron in MS immunopatterns II and III.
c) Used chemically specific imaging to differentiate between various chemical forms of iron.

My second research objective was to examine oxidative damage in active MS lesions in human MS biopsies to determine whether there are differences between lesions and PPWM. To do this, I:

a) Used histopathology to determine the demyelinating activity of lesions and to differentiate between lesions and PPWM.
b) Used XFI to localize iron, sulphur, and phosphorous in MS biopsies.
c) Used chemically specific imaging to determine the iron species present.
d) Used FTIR to localize and quantify products of oxidation.

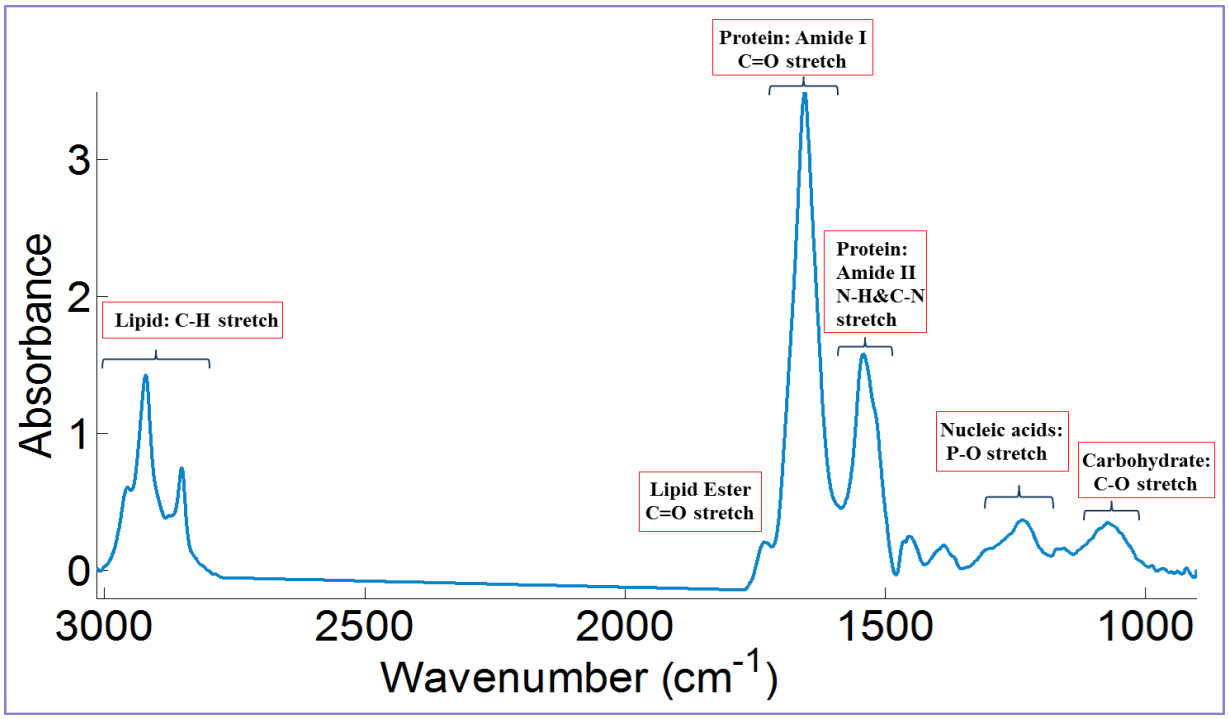

Figure 1.1 A characteristic infrared spectrum of a biological sample displaying major macromolecular functional groups.

Chapter 2 Active Lesions in Immunopatterns II and III Multiple Sclerosis Display a Differential Iron Distribution

2.1 Introduction

Significant advancements in understanding the pathogenesis of multiple sclerosis (MS), the disease's evolution, its clinical, pathological and radiological features have changed and shaped the definition of MS as a disease since the 19th century when Jean-Martin Charcot first described MS. Poser et al. postulated in 1982 that MS may not be a single disease (Poser, Raun, & Poser, 1982), but it was not until 2000 when this hypothesis was first supported by a pathological study demonstrating that early active lesions in MS are heterogeneous (Lucchinetti et al., 2000). This pathological heterogeneity suggests that the targets of injury and mechanisms of demyelination are different in disease subgroups, and classifies the lesions and the lesion-bearing MS patients in four distinct immunopatterns. Immunopatterns II and III are the most common, encompassing more than 80% of all MS patients (Lucchinetti et al., 2000), and are the focus of my study.

Iron has important roles in the central nervous system (CNS) such as the production and maintenance of myelin, and the mismanagement of iron can result in brain damage. It is presently unknown if and how iron accumulation or iron deficiency contribute to MS pathogenesis.

2.1.1. Iron in MS lesions

Oxidative stress is believed to play a significant role in the pathogenesis of MS where oxidized DNA and lipids are found in oligodendrocytes, myelin, astrocytes and axons (Haider et al., 2011). Free radicals damage subunits I and IV of the mitochondrial respiratory chain complex IV (cytochrome c oxidase; COX) and this is illustrated by the reduced expression of COX I and COX IV in oligodendrocytes, axons, and astrocytes in MS lesions (Mahad et al., 2008). Interestingly, mitochondrial defects and more severe oxidative damage are observed in immunopattern III MS lesions (Mahad et al., 2008). The oxidative stress-induced mitochondrial injury emphasizes the leakage of electrons from the respiratory chain and the production of reactive oxygen species, increase the energy demands and cause the hypoxia-like tissue damage in pattern III lesions of MS patients (Mahad et al., 2008).

What exactly causes the production of ROS and mitochondrial damage is currently debatable. One hypothesis is that microglia and macrophages produce these free radicals during

the inflammation-induced oxidative burst (Fischer et al., 2012). Another possibility is that accumulation of excess iron damages the tissues because of the iron's ability to react with oxygen and produce harmful reactive oxygen species (ROS) (Meguro et al., 2007) that cause oxidation of lipids (Haider et al., 2011; Hametner et al., 2013), proteins (LeVine & Wetzel, 1998) and DNA (Haider et al., 2011). Indeed, early research has described abnormal iron deposits in the periplaque area in MS autopsy samples but not in the control tissues suggesting that damage in MS may be related to iron accumulation (Craelius, Migdal, Luessenhop, Sugar, & Mihalakis, 1982). Defining the spatial and temporal distribution of iron is critical for understanding its role in MS pathology. LeVine (1997) et al. have demonstrated the presence of iron within macrophages in demyelinated white matter and concluded that iron accumulation at these sites may be involved in oxidative damage (LeVine, 1997). Hametner et al (2013) have compared non-heme iron in different MS plaque types and found that late active lesions contained most iron. Therefore, the distribution and content of iron may be used to differentiate among different lesion types.

Why not all CNS cells are equally affected is also uncertain. Iron in the human brain is mostly bound to ferritin and sheltered in a soluble, bioavailable form (Friedman et al., 2011; Theil, 1987). Ferrous iron enters the ferritin protein shell, is oxidized to ferric iron in the ferroxidase centres of the H-ferritin subunits, then mineralized to ferrihydrite and added to the iron core of ferritin by the L-ferritin subunits (Arosio, Carmona, Gozzelino, Maccarinelli, & Poli, 2015; Chasteen & Harrison, 1999; Theil, 2013). The deposition of the excess iron in ferritin serves as a protective mechanism by impairing the ferrous iron to participate in the Fenton reaction (Friedman et al., 2011). In addition, several molecules such as superoxide dismutase and glutathione have the ability to reduce ROS and serve as important cellular antioxidant defenses. An increased susceptibility to oxidative stress and/or an inability to properly upregulate their antioxidant defense mechanisms (van Horssen, Schreibelt, Drexhage, et al., 2008), may render the oligodendrocytes more susceptible to apoptosis in immunopattern III MS.

2.1.2. Visualizing Iron in MS

The current gold standard for visualizing iron in the brain is histochemistry. The histological demonstration of iron is performed using the Perls' and Turnbull histochemical methods, which detect ferric and ferrous iron, respectively. The Perls' staining uses acid-ferrocyanide that reacts with ferric iron to form the insoluble Prussian blue. Similarly, the Turnbull

method is based on the reaction between acid-ferricyanide and free ferrous ions (Meguro et al., 2007). The DAB enhancement of both Perls' and Turnbull's histochemical methods allows for a better visualization of iron. The study of iron in the brain has been hindered by the limitations of histochemistry: iron histochemistry cannot detect the heme iron and is not quantifiable. X-ray fluorescence imaging (XFI) addresses all the limitations of histochemistry: it is element specific, quantitatively detects all chemical forms of iron and can simultaneously map additional metals which is important when considering the relationship between iron and other chemical elements (Popescu et al., 2009a; Popescu et al., 2009b; Popescu et al., 2009c; Popescu and Nichol, 2011; Pushie et al., 2014).

Magnetic resonance imaging (MRI) has been proposed as the imaging technique of choice to detect iron *in vivo* and MRI sequences such as phase and R2* multi-gradient echo (GRE) and susceptibility weighted imaging (SWI) have been used to further the understanding of the role of iron in MS pathogenesis (Bagnato et al., 2011; Zheng, Nichol, Liu, Cheng, & Haacke, 2013; Zhong, Utriainen, Wang, Kang, & Haacke, 2014). By comparison with histochemistry, phase and R2* GRE imaging have localized iron to microglia and macrophages at the lesions' edge and to oligodendrocytes in the periplaque white matter (PPWM) (Bagnato et al., 2011; Mehta et al., 2013). Phase imaging has also been used to quantify iron in macrophages in an attempt to differentiate between macrophages associated with pro- or anti-inflammatory phenotypes within lesions (Mehta et al., 2013). Iron quantification with MRI is however unreliable because of formalin fixation, the water content, and tissue composition can influence these measurements (Zheng et al., 2013). While XFI cannot be used to detect iron *in vivo*, it should be considered the gold standard upon which new iron-sensitive and iron-specific MRI sequences are developed.

2.1.3. Hypothesis

I hypothesized that there is iron heterogeneity in MS, and that the oxidative stress that drives the mitochondrial injury and demyelination in immunopattern III MS is caused by iron accumulation.

2.2 Materials and Methods

2.2.1 Sample Preparation

Human autopsy and biopsy MS tissues were retrieved from the Department of Laboratory Medicine and Pathology, University of Saskatchewan, from the Mayo Clinic in Rochester, MN, USA, and from the University of Vienna, Austria. Tissues were fixed in 10% formalin, embedded in paraffin and sectioned with an ultra-thin semi-automatic microtome (KD-3358). Sections were floated in a 30% ethanol bath for approximately five minutes, then placed in a water bath (Leica HI 1210) set at 42-43°C. Five and 15 micrometer (µm)-thick sections were collected on glass slides and plastic coverslips (Thermanox) for immunohistochemistry and synchrotron imaging, respectively. Sections were dried overnight at room temperature.

2.2.2 Histology and Immunohistochemistry

Sections were stained with Luxol-fast blue/hematoxylin and eosin (LFB-HE) (Kluver & Barrera, 1953) to visualize myelin and H&E to visualize the tissue and cell morphology (Mallory, 1938). Immunohistochemistry was performed using an Avidin-Biotin technique on serial sections. Five µm sections were deparaffinised in xylene and rehydrated through graded alcohol. Endogenous peroxidase activity was blocked by pre-treating the sections with 3% hydrogen peroxide (30% stock H_2O_2 RICCA Chemical Co., Cat. No. 3821.7-32) in absolute methanol. Antigen retrieval was performed by immersing the sections in 10mM citric acid buffer (pH 6) and steaming them for 45 minutes in a vegetable steamer (Black and Decker). Once antigen retrieval was complete, sections were cooled and coverplated. Sections were blocked with 10% fetal bovine serum (ATCC, Cat. No. 30-2020) for 15 minutes at room temperature and incubated overnight at 4°C with the primary antibodies listed in Table 1.

Sections were then incubated for one hour at room temperature with the following biotinylated secondary antibodies diluted with 3% human serum (Cedarlane, Cat. No. H4522-100mL) in 10% FBS: donkey anti-rabbit IgG (1:200, Jackson Immuno Lab, Cat. No. 711-065-152), sheep anti-mouse IgG (1:200, GE Healthcare, Cat. No. RPN1001), and rabbit anti-goat (1:200, Jackson Immuno Lab, Cat. No. 305-65-003). Sections were then incubated with Avidin-Peroxidase (1:100, Sigma-Aldrich, Cat. No. A3151) for one hour at room temperature, followed by development with 3, 3'-Diaminobenzidine (DAB) Tetrahydrochloride Hydrate (Amresco, Cat. No. D430-10mg). The DAB reaction was stopped in tap water and sections were counterstained with Mayer's

Hematoxylin (Sigma-Aldrich, Cat. No. MHS16-500), differentiated in an acid alcohol solution (0.5% HCl in 70% ethanol) for 30 seconds, and blued in Scott's solution for 10 minutes at room temperature. This was followed by dehydration through graded alcohols to xylene and finally mounting with Cytoseal-60 (Fisher Scientific, Cat. No. 8310-4).

2.2.3. Characterization of Immunopatterns

Active lesions and periplaque white matter (PPWM) regions were identified and immunopatterned as previously described (Lucchinetti et al., 2000; Metz et al., 2014). Active lesions were demyelinated lesions infiltrated by macrophages containing myelin degradation products. PPWM was the white matter immediately surrounding the demyelinated lesions. While myelin is preserved in the PPWM, these regions often display signs of injury such as inflammation and microglial activation (Moll et al., 2011)

2.2.4. X-ray Fluorescence Imaging

Rapid scanning XFI and microprobe XFI were carried out on beam lines (BL) 10-2 and 2-3, respectively at the Stanford Synchrotron Radiation Lightsource (SSRL). Serial sections, 15 μm thick, were placed on metal free plastic coverslips (Thermo Fisher Scientific, Cat. No. 72271). On BL 10-2, whole sections were imaged at 50 μm resolution, achieved with a 50 μm pinhole aperture. The incident energy was 12.5 keV and the dwell time 80 ms per pixel. On BL 2-3, regions of interest of the samples previously imaged on BL 10-2 were scanned at 3 μm resolution, using 12.5 keV incident beam focused with Kirkpatrick-Baez (KB) focussing mirrors. Data was collected with a 120 ms dwell time per pixel. The samples were mounted vertically at 45° to the incident X-ray beam and 45° to the detector, and continuously raster scanned in the beam.

2.2.5 Chemically Specific Imaging

Chemically specific imaging was performed at BL 2-3 to differentiate between various iron species in small regions of interest. Data was collected at incident energies of 7118.5 eV, 7126.5 eV, and 7132 eV for iron-sulfur clusters, ferrous and ferric iron, respectively, using five μm resolution and 100 ms dwell time

Table 2.1 Primary antibodies used for immunohistochemistry.

Protein target	Species	Dilution	Source	Catalogue Number
Proteolipid protein (PLP)	Mouse	1:500	AbD Serotec	MCA839G
Myelin-associated glycoprotein (MAG)	Rabbit	1:500	Sigma-Aldrich	HPA012499
Myelin oligodendrocyte glycoprotein (MOG)	Rabbit	1:1000	Abcam	ab109746
CD68	Mouse	1:100	DakoCytomation	M0879
Heavy chain ferritin (HF)	Rabbit	1:1000	Abcam	ab65080
Light chain ferritin (LF)	Goat	1:300	Abcam	ab110017
Transferrin (TF)	Rabbit	1:1000	Sigma-Aldrich	HPA005692
Transferrin receptor (TFRC)	Rabbit	1:500	Sigma-Aldrich	HPA028598
Complement C9neo antigen (C9neo)	Mouse	1:200	Professor Morgan from Cardiff, UK	Clone B7
Terminal complement complex (TCC) and C9	Rabbit anti-human	1:200	Professor Morgan from Cardiff, UK	-
Terminal complement complex (TCC) and C9	Rabbit anti-rat	1:200	Professor Morgan from Cardiff, UK	-

2.2.6 Image Analysis

The XFI images were generated using Microanalysis Toolkit (Samuel Webb, SSRL; http://www.sams-xrays.com/smak). All images were normalized to I0 to account for variations in the incoming beam intensity. SMAK was also used to quantify iron content in the samples.

2.2.7 Iron Quantification

Histology slides were scanned at 40x magnification using an Olympus VS110 virtual slide scanner microscope. Whole maps were saved as .jpeg files on which regions of interest of active lesions and PPWM were identified and outlined. XFI images were generated using Microanalysis Toolkit. Histology and XFI maps were displayed side by side, and the regions of interest were masked on the XFI maps using the histology maps as guides. Values for iron from each mask were collected for further statistical analyses.

2.2.8 Statistical Analysis

Statistical analysis was performed at the Mayo Clinic. Comparisons of pattern II vs. pattern III were carried out using generalized estimating equations (GEE) models with an 'exchangeable' correlation structure in order to take into account that regions from the same subject are likely to be correlated. The metal values were log transformed in order to assist with the interpretation of the model output. Analyses using untransformed metal values yielded similar results.

2.3 Results

2.3.1 Pathological Characteristics of Immunopatterns II and III

Nine cases were classified as immunopattern II (Fig. 2.1) and 18 cases as immunopattern III (Fig. 2.2). Lesions in both immunopatterns II and III were infiltrated by activated macrophages/microglia (Fig. 2.1D, and E, 2.2D, and F). Important histological features of immunopattern II lesions included complement activation onto myelin sheaths (Fig. 2.1G, *arrows*) and within macrophages (Fig. 2.1H, *arrows*), which was not observed in immunopattern III lesions (Fig. 2.2E). Immunopattern III lesions showed preferential loss of MAG compared to PLP (Fig. 2.2B and C), while all myelin proteins were equally lost in immunopattern II MS (Fig. 2.1B and C).

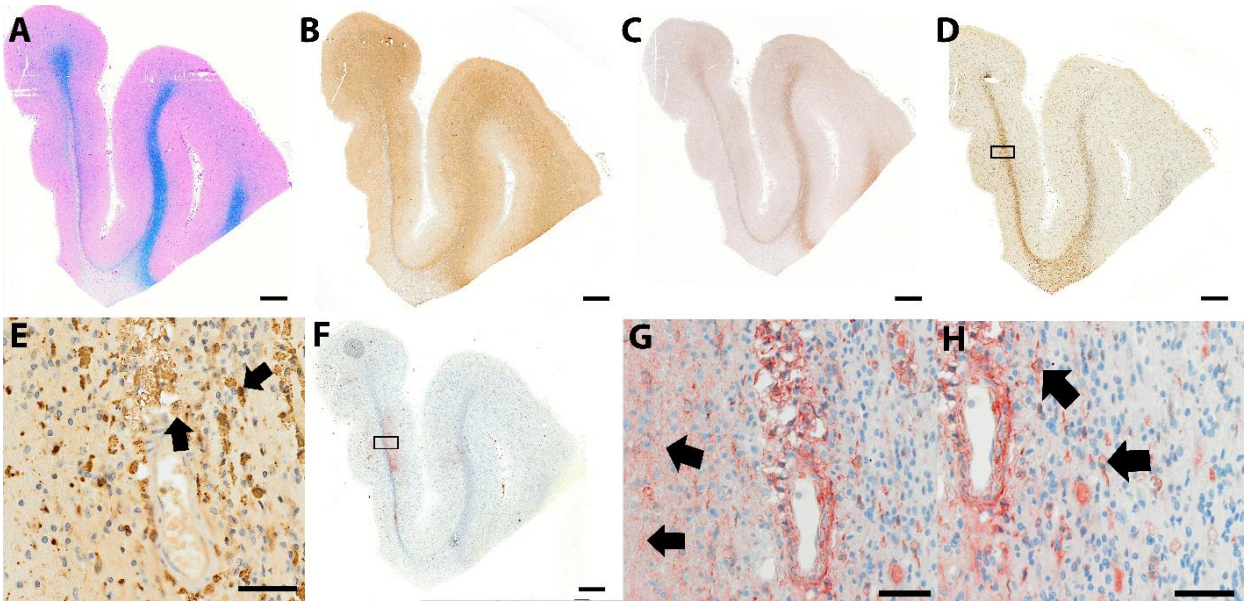

Figure 2.1 Activation of complement on myelin and within macrophages and equal loss of myelin proteins are characteristic for immunopattern II MS lesions. The demyelinated lesion is illustrated by the (A) absence of the blue histological stain (LFB-HE), as well as the lack of immunoreactivity for (B) proteolipid protein (PLP) and (C) myelin-associated glycoprotein (MAG). D. Macrophages infiltrate the demyelinated lesion (KiM1P). E) At higher magnification, foamy macrophages (*arrows*) are seen perivascularly and in the surrounding tissue (KiM1P). F) The activation of complement is a hallmark feature of pattern II MS lesions. Higher magnification shows that activated complement is localized on myelin sheaths (G, *arrows*) and within macrophages (H, *arrows*). Scale bar: (A-D, F) 2 mm; (E, G & H) 50 µm.

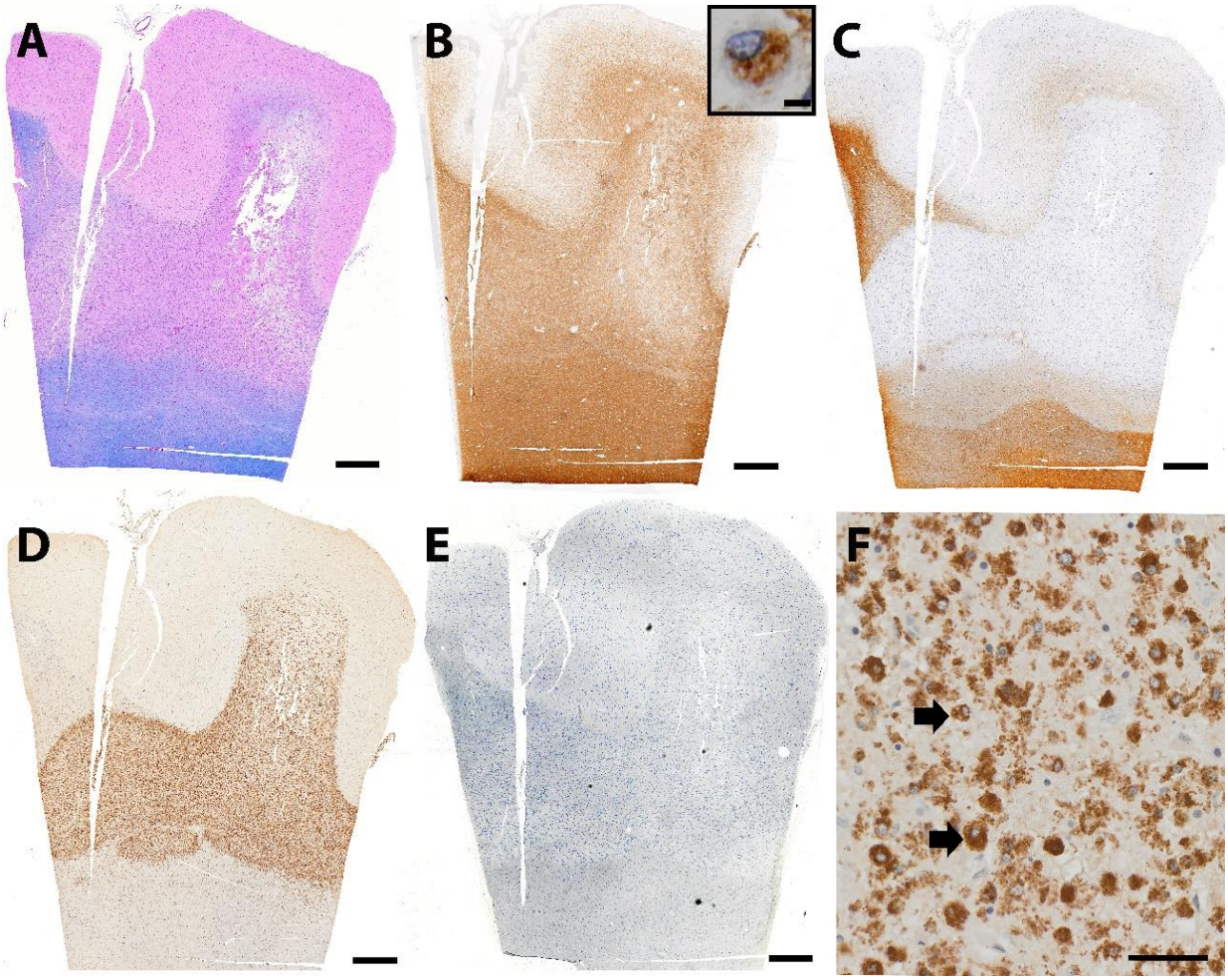

Figure 2.2 Preferential loss of myelin-associated glycoprotein and the preservation of other myelin proteins is characteristic for immunopattern III MS lesions. A) The demyelinated lesion is illustrated by the absence of the blue histological stain (LFB-HE). B) Proteolipid protein (PLP) is relatively preserved, but PLP debris is seen within macrophages (inset). C) Myelin-associated glycoprotein is preferentially lost (MAG). D) Macrophages infiltrate the demyelinated lesion (KiM1P). E) Activation of complement is absent (C9neo). F) High magnification shows the sea of macrophages (*arrows*) within the lesion (KiM1P). Scale bar: A-E) 2 mm; F) 50 µm; inset in B) 5 µm

2.3.2 Immunopattern II Lesions Contained More Iron Than Immunopattern III Lesions and Iron Localized Within Macrophages

Rapid-scanning XFI showed that immunopattern II MS lesions (Fig. 2.3B) contained more iron than immunopattern III MS lesions (Fig. 2.3F), and this difference attained statistical significance (p=0.003) (Fig. 2.4). The difference between the iron content of the PPWM in immunopatterns II and III was not significantly different (p=0.16). Immunopattern II lesions had more iron than immunopattern II PPWM (Fig. 2-3B), while iron was decreased in immunopattern III MS lesions when compared to immunopattern III PPWM (Fig. 2-3F). This distribution was also reflected in the high resolution iron maps for immunopattern II (Fig. 2.3C and D), and immunopattern III (Fig. 2.3G and H), respectively. Micro-focused X-ray fluorescence showed that iron in immunopattern II localized to discrete structures (Fig. 2.3C), identified as macrophages when iron maps were compared to the adjacent immunohistochemical-stained sections. These macrophages also contained intracytoplasmic granules immunoreactive for myelin and complement (Fig. 2.2B inset and 2.1H). Myelin-laden macrophages in active immunopattern III lesions did not contain iron (Fig 2.3G). The PPWM of both patterns showed a patchy distribution of iron (Fig. 2.3D and H) consistent with the iron being localized to oligodendrocytes (Connor & Menzies, 1996; Todorich et al., 2009).

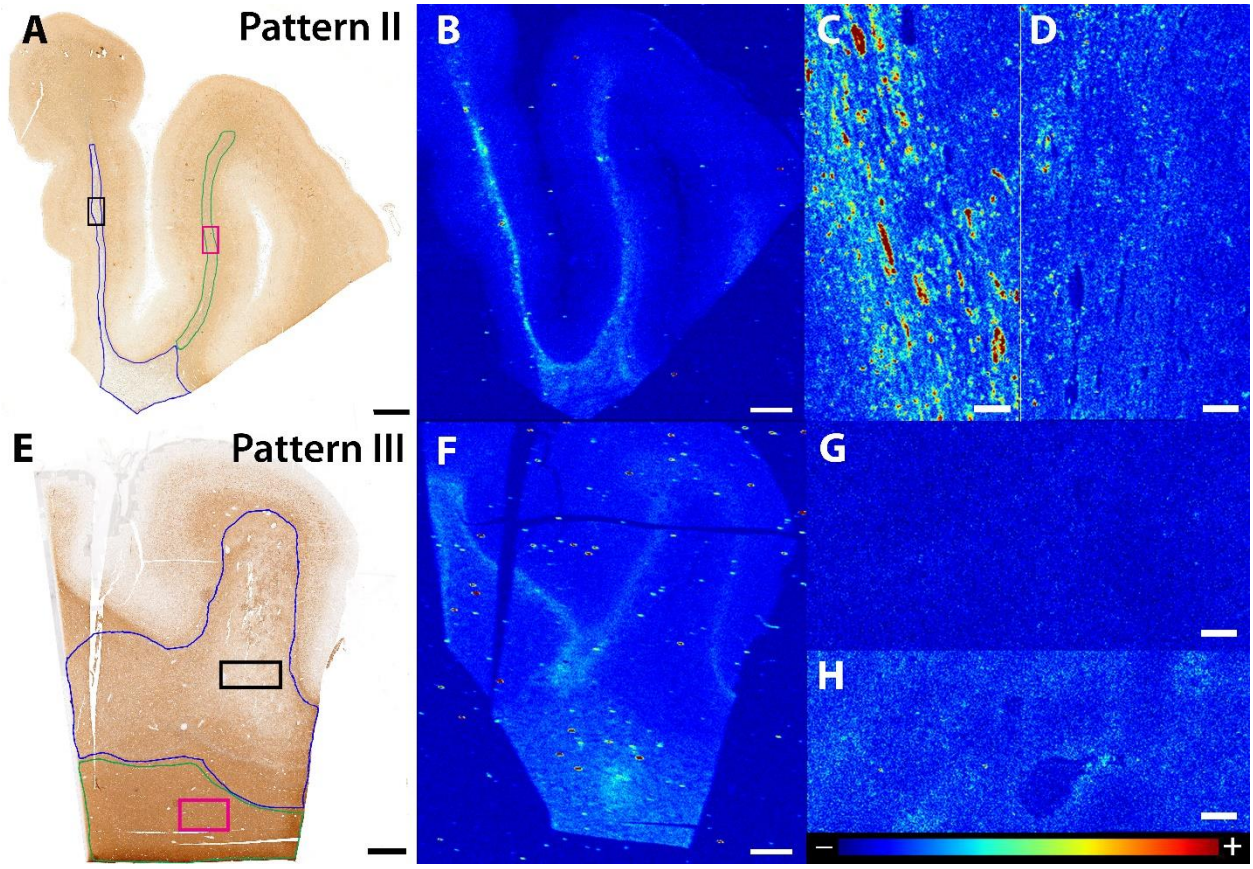

Figure 2.3 Immunopattern II lesions contain more iron than immunopattern III lesions and iron localizes to macrophages. Immunohistochemical maps of immunopattern II (A) and III (E) MS show the demyelinated lesions (blue outlines) and the PPWM regions (green outlines). Rapid-scanning XFI shows increased iron in the active lesion of immunopattern II (B), but not immunopattern III (F) MS. High resolution XFI shows that iron is localized within macrophages in immunopattern II lesions (C) while iron in the PPWM has a patchy appearance (D). High resolution XFI shows absence of iron in immunopattern III lesions (G), while iron in the PPWM has a patchy appearance (H). Intensity scale bars represent the normalized total Kα fluorescence counts, proportional to total metal present, from blue (lowest) to red (highest). Scale bar: A, B, E, F) 2 mm; C, D, G, H) 90 μm.

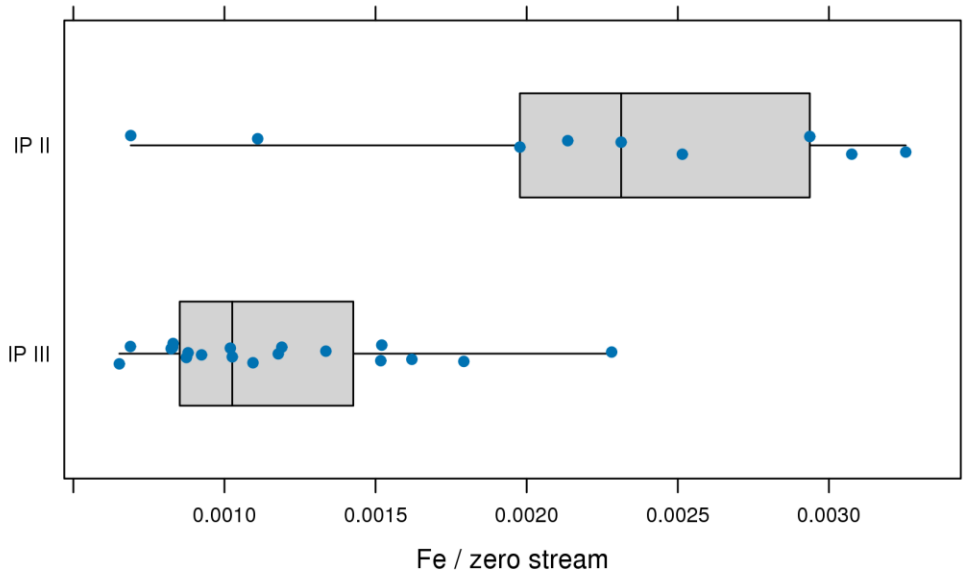

Figure 2.4 Statistical analysis of iron in active lesions show more iron in immunopattern II lesions. Iron levels were significantly higher in immunopattern II lesions (IP II) as compared to immunopattern III lesions (IP III). Estimate (95% CI): 0.56 (0.19, 0.94); p =0.003.

2.3.3 Ferric Iron is the Predominant Iron Species in Macrophages

Chemically specific imaging of iron showed that the ferrihydrite of ferritin (ferric iron coordinated with six oxygen atoms) is the predominant iron species in all samples. Ferrihydrite was most abundant in immunopattern II lesions (Fig. 2.5C), followed by the PPWM of immunopattern II (Fig. 2.5F) and immunopattern III (Fig. 2.5L) MS, and immunopattern III lesions (Fig. 2.5I). Fe-S clusters (Fig. 2.5A, D, G, and J) and ferrous iron (Fig. 2.5B, E, H, K) were unremarkable in lesions and PPWM of both immunopatterns.

2.3.4 H-Ferritin Localizes to Nuclei of Oligodendrocytes in PPWM of Immunopattern III Lesions

Both H-ferritin and L-ferritin were localized to the cytoplasm of macrophages in immunopattern II and III MS lesions (Fig. 2.6A, C, E, and G), while L-ferritin mainly stained the microglia in the PPWM of both immunopatterns (Fig. 2.6D and H). Immunoreactivity for H-ferritin in the PPWM was different between the two immunopatterns. In immunopattern II PPWM, H-ferritin immunoreactivity was identified in the cytoplasm of oligodendrocytes as a brown rim around the nuclei (Fig. 2.6B, *arrows*), while in immunopattern III PPWM, H-ferritin immunohistochemistry stained the nuclei of oligodendrocytes (Fig. 2.6F, *arrows*). Oligodendrocyte counting showed that immunopattern II cases had an approximately 10-fold increase in the odds of having no immunoreactivity to H-ferritin in the nuclei [95% CI, 11.30 (6.33, 21.41), $p<0.001$).

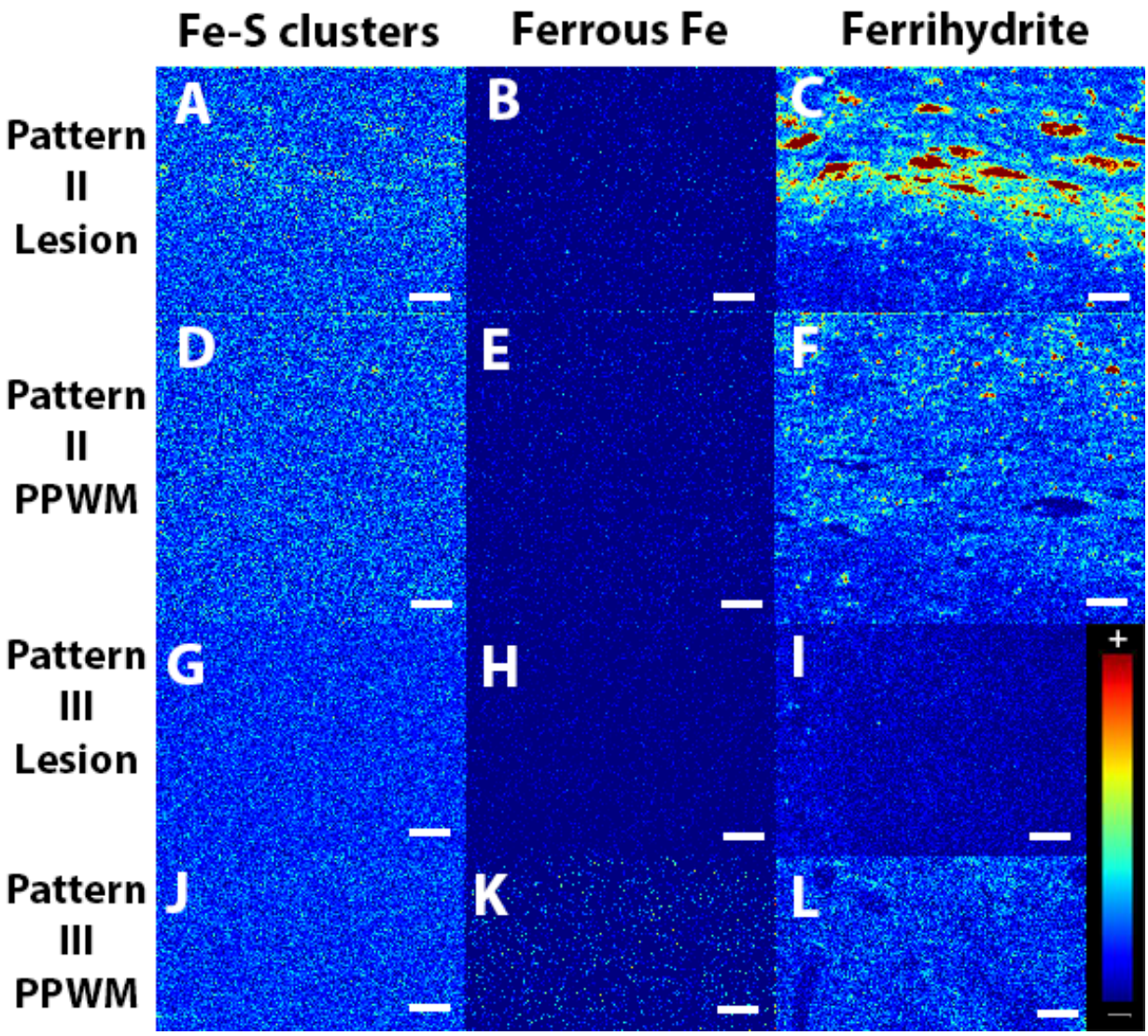

Figure 2.5 Ferrihydrite of ferritin is the predominant iron species in all samples and is highest in immunopattern II lesions. Iron-sulfur clusters (A, D, G, J) and ferrous iron (B, E, H, K) are negligible constituents of the overall iron environment in lesions (A, B, G, H) and PPWM (D, E, J, K) of both immunopattern II (A, B, D, E) and immunopattern III (G, H, J, K) MS. The ferrihydrite of ferritin is prominent and localized to macrophages immunopattern II lesions (C). Ferrihydrite in immunopattern II (F) and III (L) PPWM shows a patchy distribution consistent with localization to oligodendrocytes. The ferrihydrite is lowest in immunopattern III lesions (I) consistent with an iron deficient environment. Intensity scale bar represents the normalized total Kα fluorescence counts, proportional to total metal present, from blue (lowest) to red (highest). Scale bar 100 µm.

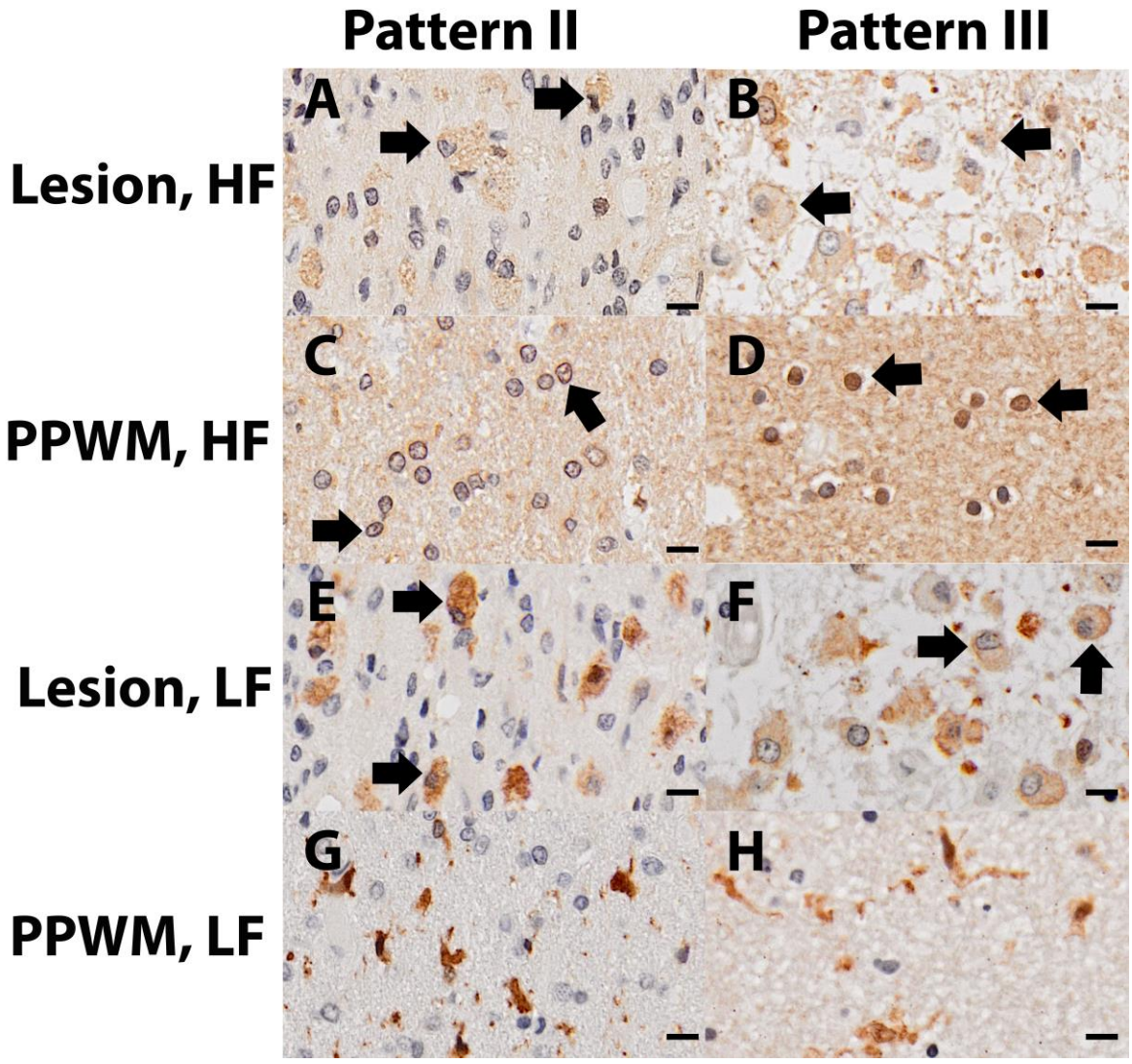

Figure 2.6 Ferritin heavy chain (H-ferritin) localizes to oligodendrocyte nuclei in immunopattern III PPWM, and to the cytoplasm of oligodendrocytes in immunopattern II PPWM. H-ferritin is seen (A) in the cytoplasm of macrophages (*arrows*) in the immunopattern II lesion (HF), and (B) in the cytoplasm of oligodendrocytes (arrows) in immunopattern II PPWM (HF). L-ferritin immunoreactivity is positive (C) in the cytoplasm of macrophages (arrows) in immunopattern II lesion (HF) and (D) within microglia of immunopattern II PPWM (LF). H-ferritin localizes (E) to the cytoplasm of macrophages (*arrows*) in immunopattern III lesions (HF) and (F) to oligodendrocyte nuclei (*arrows*) in immunopattern III PPWM (HF). L-ferritin stains (G) macrophages (*arrows*) in immunopattern III lesions (LF) and (H) microglia in immunopattern III PPWM (LF). Scale bar: 10 µm; HF – H-ferritin; LF – L-ferritin.

2.4 Discussion

This study shows that the pattern of iron is distinct and heterogeneous across different MS immunopatterns. Using cutting edge X-ray fluorescence synchrotron imaging that is sensitive and specific to iron (Pushie et al., 2014), I report for the first time that the distribution and content of iron differs between immunopatterns II and III MS lesions. It has been previously suggested that macrophages and microglia in early MS accumulate iron that is released from destroyed oligodendrocytes (Hametner et al., 2013). However, while macrophages were present and abundant in both immunopattern II and III active MS lesions, only those present in immunopattern II lesions accumulated iron. This indicates that there may be more factors, in addition to the previously suggested iron storage shift from destroyed oligodendrocytes to macrophages and microglia, that affect how macrophages accumulate or release iron.

One possibility is that this heterogeneous iron loading of macrophages reflects their different polarization states (Corna et al., 2010; Mehta et al., 2013). Polarization is a spectrum of functional profiles that macrophages adopt depending on signals they receive from the immune cells. At one end of the spectrum, classically activated (or M1-polarized) macrophages are pro-inflammatory while at the opposing end of the spectrum, alternatively activated (or M2-polarized) macrophages help resolve inflammation (Cairo, Recalcati, Mantovani, & Locati, 2011). M1 macrophages, associated with the production of ROS and pro-inflammatory cytokines, sequester iron (Gammella, Buratti, Cairo, & Recalcati, 2014). M2 macrophages export iron out of the cell and decrease their ferritin levels (Gammella et al., 2014). This reduces the intracellular iron availability therefore blocking the formation of iron-dependent enzymes involved in the inflammatory response with dampening of inflammation, and increases the extracellular iron availability which helps to promote tissue repair (Cairo et al., 2011). Such an iron-related macrophage polarization dichotomy has been previously described, but attributed not to different mechanisms of demyelination but to the ability of macrophages to phagocytose iron and myelin: macrophages accumulate iron and this induces a pro-inflammatory M1-polarization state, while myelin ingestion prevents M1-polarization and iron uptake and converts macrophages to an anti-inflammatory M2-polarization state (Mehta et al., 2013).

Another possibility is that the iron heterogeneity of macrophages is an expression of the different mechanisms of demyelination postulated to occur in these two different MS

immunopatterns. Demyelination in immunopattern II MS is hypothesized to be caused by complement activating antibodies that target yet unknown antigens on oligodendrocytes and/or myelin. Accordingly, there is a striking co-localization of antibody deposition and complement activation on myelin in immunopattern II MS (Lucchinetti et al., 2000). Specifically, deposition of the complement component C1q and activation of the terminal lytic complex C5b-9 is seen within myelin-laden macrophages and on abnormal myelin in MS active lesions (M. H. Barnett, Parratt, Cho, & Prineas, 2009; Lucchinetti et al., 2000; Storch et al., 1998). C1q is responsible for tagging foreign pathogens and subsequently triggering the classical complement pathway that leads to destruction of the pathogen, and in the presence of ferrous iron ions, C1q increases its binding to immunoglobulins (Dimitrov, Roumenina, Doltchinkova, & Vassilev, 2007). C5 is also known to bind iron ions and iron is required for the conversion of C5 to activated C5b by hydroxyl radicals (Vogi, Nolte, & Brunahl, 1991). C5b interacts with other complement components to form C5b-9, which is the membrane attack complex (MAC) that forms the transmembrane pores that kill the targeted cell (Tegla et al., 2009). Thus, iron is essential for complement function and terminal lytic complex assembly, explaining why immunopattern II MS macrophages that phagocytose complement-opsonized myelin debris contain increased amounts of iron.

In contrast to the high iron content of macrophages in immunopattern II, macrophages in immunopattern III MS lesions contained very little iron. Oxidative stress and mitochondrial injury play an important role in the pathogenesis of immunopattern III MS (Haider et al., 2011; Mahad et al., 2008) and it has been assumed that excess iron drives the tissue injury in immunopattern III MS (Hametner et al., 2013). My results however show that iron deficiency, rather than the excess of iron, drives the pathology of immunopattern III lesions. Iron is essential for energy production because it functions as a cofactor for cytochromes a, b, c, and Fe-S clusters of the mitochondrial respiratory chain (Todorich et al., 2009). Depletion of iron, as observed in immunopattern III lesions, can cause mitochondrial dysfunction by disrupting the iron-sulfur cluster biogenesis and production energy leading to a state of virtual hypoxia that would primarily affect demyelinated axons requiring an increased energy demand to maintain nerve conduction (Trapp & Stys, 2009). The disruption of oxidative phosphorylation also causes an increase rate of electron escape from the mitochondrial respiratory chain resulting in increased ROS production (Higgins et al., 2010) with oxidation of phospholipids and DNA (Haider et al., 2011). Mitochondrial dysfunction can activate apoptotic pathways (Zhang et al., 2005) and the immunopattern III-characteristic

oligodendrocyte apoptosis (Aboul-Enein et al., 2003). This is also reinforced by the finding that, unlike oligodendrocytes in immunopattern II PPWM where H-ferritin is expressed in the cytoplasm, the H-ferritin in immunopattern III PPWM oligodendrocytes is localized to the nuclei. This is consistent with the translocation of H-ferritin from the cytoplasm to the nuclei of oligodendrocytes where it binds to the DNA in order to protect it from ROS-induced damage (Alkhateeb & Connor, 2010; Thompson, Fried, Ye, Boyer, & Connor, 2002).

The most important study limitation is the use of formalin-fixed paraffin embedded tissue equally affecting both iron histochemistry and XFI. Formalin fixation is routinely used in pathology labs to preserve the tissue and prevent decomposition and autolysis (Thavarajah, Mudimbaimannar, Elizabeth, Rao, & Ranganathan, 2012) and is known to leach metals from tissues, although its extent is debatable (Bush, Moyer, Batts, & Parisi, 1995; Chua-anusorn, Webb, Macey, Pootrakul, & St Pierre, 1997; Schrag et al., 2010). It is expected that the paraffin embedding process accentuates this leaching phenomenon through the exposure of tissues to alcohol, xylene and increased temperatures. The paraffin embedding process also oxidizes metals explaining perhaps why no ferrous iron was detected and raising questions about the ability of Turnbull stain to exclusively detect ferrous iron in formalin fixed paraffin embedded tissue sections (Hackett et al., 2011).

MS is heterogeneous with respect to clinical, genetic, radiographic, and pathologic features, and it seems increasingly plausible that MS may be a cluster of diseases with similar clinical presentation. The challenge is now to identify surrogate MRI, clinical, genetic, serological and/or CSF markers that would correlate with immunopatterns in the non-biopsied MS patient population. I show here that lesions in immunopattern II MS contain significantly more iron than lesions of immunopattern III MS, and this novel observation paves the way for developing new or using existing iron-sensitive MRI techniques (Bagnato et al., 2011; Haacke et al., 2009) to stratify the patients with early MS. Future studies will have to validate such iron-sensitive MRI techniques by comparing the MRI with the XFI of formalin fixed brain slices (Popescu et al., 2009; Zheng et al., 2013).

The obvious practical application of the heterogeneity concept is the design of novel therapeutic strategies specifically tailored to each immunopattern. In support of this hypothesis, immunopattern II MS has been shown to be uniquely responsive to plasma exchange for treatment

of steroid unresponsive fulminant MS relapses, while this treatment does not benefit either immunopattern I, or immunopattern III MS patients (Keegan et al., 2005). The proposal of iron chelation therapy in MS is controversial (Creange, Lefaucheur, Balleyguier, & Galacteros, 2013; Stephenson et al., 2014; Weigel, Lynch, & LeVine, 2014), and stems from the premise that iron accumulates in MS lesions. Currently, there are three approved iron chelators for therapeutic use: deferoxamine, deferasirox, and deferiprone (Weigel et al., 2014). Only deferoxamine has been tested in human MS patients and the outcome of the most recent study has reported that one out of nine study patients improved, while the disability of five patients worsened (Lynch, Fonseca, & LeVine, 2000). My results also argue against indiscriminate iron chelation in all patients with early acute MS. Chelation therapy may be beneficial in immunopattern II MS where it would decrease the C1q binding to the antibodies and impair the cleavage of C5 therefore impeding the formation of the terminal lytic complex and protecting oligodendrocytes and myelin. However, the chelation of the minimal amounts of iron present in immunopattern III MS lesions may supress the already challenged metabolic activity of oligodendrocytes thereby accelerating their death (Zhang et al., 2005).

Chapter 3 Oxidative Injury in Active Multiple Sclerosis Lesions

3.1 Introduction

Multiple sclerosis (MS) is a disease of the central nervous system (CNS) that causes disability in young people between the ages of 15 and 40 and is twice as likely to occur in females than males (Hader & Yee, 2007; MS Society of Canada, 2016). In MS, the oligodendrocyte and its product, the myelin sheath protecting axons, are targeted and destroyed by the body's immune system leading to the formation of demyelinated plaques or lesions. Pathological features of MS change over time and differ in the early versus chronic phases of the disease (Popescu et al., 2013). Active lesions predominate in early, relapsing remitting MS, but decline to nearly zero percent in long-standing chronic progressive MS where inactive lesions become predominant. Therefore, the active lesion is the earliest pathological change occurring in MS and represents the pathological substrate of attacks in relapsing-remitting MS (RRMS) (Frischer et al., 2015). This shows the complex and dynamic nature of MS and reinforces the idea that MS is not driven by a single mechanism of action that only one therapeutic strategy can solve. For example, anti-inflammatory, immunomodulatory, or immunosuppressive therapies tend to benefit patients in the early phase of the disease more than patients who are in the progressive stage (Lassmann et al., 2007).

3.1.1 Oxidative Injury and MS

The brain is highly susceptible to oxidative injury due to its high concentrations of lipids and unsaturated fatty acids (Friedman et al., 2011). Lipid peroxidation occurs when a reactive oxygen species (ROS) takes an electron from an unsaturated fatty acid in the lipid membrane, resulting in an unstable lipid radical that can react in a chain reaction with oxygen to form lipid hydroperoxides (McGill & Jaeschke, 2013). Oxidative stress is believed to play a significant role in the pathogenesis of MS: oligodendrocytes have been shown to be more vulnerable to oxidative stress than other glial cells *in vitro* (Mitrovic, Ignarro, Montestruque, Smoll, & Merrill, 1994); the highly toxic end product of lipid oxidation, 4-hydroxy-2-nonenal (HNE), is increased in demyelinated MS lesions compared to the periplaque white matter (PPWM) (van Horssen et al., 2008) and oxidized phospholipids are localized to myelin, oligodendrocytes, and acutely injured axons in actively demyelinating lesions (Haider et al., 2011). Severe oxidative damage to cell membranes can trigger cell death by apoptosis or necrosis (Fuchs, Perez-Pinzon, & Dave, 2014),

which may explain the characteristic immunopattern III MS oligodendrocyte apoptosis (Lucchinetti et al., 2000).

Oxidative stress is more commonly seen in immunopattern III MS lesions, which are characterized by a distinctive loss of myelin-associated glycoprotein (MAG) compared to other myelin proteins such proteolipid protein (PLP), myelin basic protein (MBP) or myelin oligodendrocyte glycoprotein (MOG). MAG is a transmembrane glycoprotein that is located in the innermost layer of the myelin sheath surrounding the axon and plays an important role in oligodendrocyte-axon interactions (Quarles, 2007). Its preferential destruction is hypothesized to be the result of metabolic disturbances in oligodendrocytes (Popescu & Lucchinetti, 2012b) indicating "dying-back" oligodendrogliopathy, in which the earliest pathological changes occur in the oligodendrocyte processes distal to the cell body. Oligodendrocytes are highly metabolic cells that require much energy in the form of adenosine triphosphate (ATP), which is produced in mitochondria (Todorich et al., 2009). Important mitochondrial proteins involved in oxygen consumption and ATP synthesis have been shown to be defective in MS lesions (Mahad et al., 2005), and this oxidative damage –induced mitochondrial injury is postulated to drive tissue injury in MS (Haider et al., 2011). Mitochondria produce ROS normally as a by-product of cellular respiration, but only when the production of ROS overwhelms the antioxidant system, does ROS mediate oxidative damage to membrane lipids, deoxyribonucleic acid (DNA), and proteins (van Horssen et al., 2008).

The oligodendrocyte is the CNS cell that stains most robustly for iron and many of the enzymes involved in ATP synthesis, and in the synthesis of cholesterol and lipids integral for the myelin's composition use iron as a cofactor (Todorich et al., 2009). Excess cellular iron is safely stored as ferric iron in ferritin (Hulet et al., 1999) to protect the cell from the redox-active ferrous iron, which can form toxic ROS via the Fenton reaction (Hametner et al., 2013). It has been suggested that destruction of iron-rich myelin and oligodendrocytes in MS lesions leads to a liberation of iron into the extracellular space, propagating a wave of iron-induced oxidative damage (Hametner et al., 2013).

Elemental sulphur is a component of sulfatides, which are important constituents of myelin (Stuber et al., 2014). Sulphur is also part of many enzymes and antioxidant molecules, such as glutathione (Mukwevho et al., 2014). Oligodendrocytes and endothelial cells in MS lesions have

been shown to have low levels of antioxidant enzymes, which may render oligodendrocytes more susceptible to oxidative damage (van Horssen et al., 2008). Sulfur is also an important component of Fe-S clusters, which are involved in crucial cell functions such as respiration, catalysis, and redox reactions (Todorich et al., 2009; Ye & Rouault, 2010), and improper Fe–S cluster protein formation can lead to iron overload in mitochondria in mammalian cells (Rouault, 2012).

Myelin is made of 70% lipids in the form of cholesterol, galactolipid, and phospholipid (Stuber et al., 2014), and about 80% of phosphorous in white matter and 60% in gray matter is located in phospholipids (Stuber et al., 2014), providing a good biomarker for myelin health in MS. Phospholipids, and cholesterol are particularly vulnerable to oxidative damage (Ayala, Munoz, & Arguelles, 2014). Phosphorous is also found in DNA in phosphomonoester and phosphodiester proteins. Phosphocreatine and nucleoside phosphates like ATP and adenosine diphosphate (ADP), important in energy transfer, contain phosphorous.

Reactive oxygen species causing mitochondrial injury may be an important tissue injury mechanism. Oxidized lipids and proteins stand as oxidative damage markers. The lack of techniques, which can reliably quantify and image such biochemical species, has been a long-standing obstacle to the study of oxidative stress contribution to MS. To date, the most convincing data showing tissue oxidative damage has been acquired immunohistochemically (Haider et al., 2011). However, this approach leads to false-positive results, lacks quantification sensitivity and specificity as it is based on staining densitometry, and fails to identify all oxidized proteins and lipids.

Characteristic marker bands for oxidized lipids and proteins are present in Fourier transform infrared (FTIR) spectra. FTIR microspectroscopy is a technique suitable to study such biological processes in situ due to the wealth of molecules which absorb light across the mid-infrared range (Caine et al., 2012). As the technique is non-destructive, it is easily compatible with histology. Oxidative damage in MS lesions has been studied in the past using infrared spectroscopy (Choo et al., 1993; LeVine & Wetzel, 1998). One study used autopsy samples from MS patients to detect and localize free radical damage in active MS lesions, but did not provide either the demyelinating staging or the criteria used to classify active lesions (LeVine & Wetzel, 1998). Despite detecting tissue oxidative damage it is not clear at which stage of MS lesion development the reported changes take place. Past studies often had to rely on autopsy tissues collected from

patients in the chronic stage of the disease (De Groot et al., 2001) leaving a gap in information about pathological processes occurring at the onset of MS. A brain biopsy is the removal of brain tissue from a living patient for immediate pathological examination. Although brain biopsies are rarely used as part of MS diagnosis, they are sometimes performed to exclude other pathologies like tumours (Kuhlmann, Lassmann, & Bruck, 2008). Biopsy samples are often collected from MS patients near the first symptom onset, during the first demyelinating episode and present a novel opportunity to study the involvement of oxidative damage in the earliest demyelinating stages. To my knowledge, this is the first FTIR study performed on MS brain biopsy tissues.

3.1.2. Aim of Study

My hypothesis is that oxidative damage to lipids and proteins is present in the earliest MS lesion stages. The aim of this study is to analyze the role of oxidative stress in the pathology of MS.

3.2 Materials and Methods

3.2.1 Sample Preparation

Six patient biopsies with the diagnosis of demyelination consistent with MS confirmed by a certified neuropathologist were retrieved from the Department of Laboratory Medicine and Pathology of the Saskatoon Health Region. Five, ten, and fifteen micron-thick sections were cut with an ultra-thin semi-automatic microtome (Zhejiang Jinhua Kedi Instrumental Equipment Co., KD-3358). Sections were floated in a 30% ethanol bath for approximately five minutes, then placed in a water bath (Leica HI 1210) set at 42-43°C. Five micron-thick sections were collected on glass slides for histology and immunohistochemistry. Ten micron-thick sections were collected on calcium fluoride optical windows for mid-infrared imaging and fifteen micron-thick sections were collected on metal-free plastic coverslips for X-ray fluorescence imaging. These were left to dry overnight at room temperature.

3.2.2 Histology and Immunohistochemistry

Sections were stained with Luxol-fast blue/hematoxylin and eosin (LFB-HE) (Kluver & Barrera, 1953), H&E (Mallory, 1938), Bielschowsky silver impregnation (Yamamoto & Hirano, 1986), and a modified Turnbull staining protocol (Meguro et al., 2007). Immunohistochemistry was performed using an Avidin-Biotin technique as detailed in chapter 2, section 2.2.

3.2.3 X-ray Fluorescence Imaging

Rapid scanning microfocused XFI was performed on beamlines 2-3 and 14-3 at the Stanford Synchrotron Radiation Lightsource (SSRL). Fifteen μm-thick samples collected on plastic coverslips were mounted onto a motorized stage oriented at 45° to the incident beam. Beamline 2-3 was used to examine iron (6210 – 6700 eV) with an incident energy of 12.5 keV, a spot size of 3 μm x 3 μm and a dwell time of 120 ms/point. Beamline 14-3 was used to image sulphur (2260 – 2360 eV) and phosphorous (1960 – 2060 eV) with an incident energy of 4.25 keV, a 5 μm x 5 μm spot size and a dwell time of 50ms/point.

3.2.4 Chemically Selective Imaging

Chemically selective imaging was carried out on beamline 2-3 at five-micron resolution and using a dwell time of 100 ms. Images were collected at incident energies of 7118.5 eV, 7126.5 eV, and 7132 eV corresponding to Fe-S clusters, ferrous iron, and ferric iron, respectively.

3.2.5 Fourier-transform Infrared Microspectroscopy

FTIR imaging was performed on the MidIR beamline at the Canadian Lightsource (CLS) using the Hyperion 3000 FTIR imaging system (Bruker Optics, Ettlingen, Germany) that is equipped with a liquid nitrogen cooled 64 x 64 Mercury-Cadmium-Telluride (MCT) focal plane array (FPA) detector with a 15X magnification. The spectral resolution was set to 4 cm^{-1} and the data were acquired in transmission mode. Each individual element of the array detector sampled an area approximately 2.7 x 2.7 μm^2. Pixel binning (8x8) was applied so that a larger area of the sample could be imaged and 128 scans were collected per pixel. The experiments were performed at room temperature and data were collected using the Bruker spectrometer software, OPUS. Before imaging the sample, a background spectrum was collected from the slide absent of the sample. The final absorbance spectra were calculated from the ratio of the background spectra / sample spectra. The benefits of using ratios are that it can eliminate the variability from sample thickness and also helps to overcome problems arising from spectral pre-processing.

Infrared images were generated using the ratio of the integrated area of absorption bands of interest. The protein infrared images used the integrated area under the amide I region (1700 – 1600 cm^{-1}): 1660 – 1650 cm^{-1} for alpha helices and 1635 – 1620 cm^{-1} for beta sheets. The area of 3000 – 2800 cm^{-1} is associated with the C-H stretches of lipids. The lipid oxidation infrared image was generated using the ratio of the integrated area of CH_2 (2895-2946 cm^{-1}) and CH_3 (2895-3000

cm^{-1}). The CH_3 absorption band (2958 cm^{-1}) was normalized to observe the changes in the acyl chain upon oxidation. The ester carbonyl band associated with lipid ester was at 1740 cm^{-1}. The infrared image of phosphate used the integrated area of anti-symmetric stretches of phosphate at 1280 – 1200 cm^{-1}.

3.2.6 Image Analysis

XFI image analysis was performed using Sam's Microanalysis Toolkit (SMAK; Open Source, Samuel Webb, SSRL, Stanford, CA, USA). All images were normalized to I0 to account for variations in incoming beam intensities. XFI data were not quantified in this study.

All FTIR spectral processing and classifications were carried out using OPUS software (Version 7.2, Bruker, Ettingen, Germany), and Cytospec software (Cytospec, version 2.00.01). All the spectra were preprocessed and the water vapor contribution was subtracted. In order to eliminate any intensity variation caused by changes in the thickness of the tissue, the spectra were normalized. Baseline correction was done with software Cytospec by using polynomial fitting.

3.2.7 Statistical Analysis

The paired t test was used to assess the differences in markers of oxidative stress between the lesions and PPWM. The p-values shown did not account for the SDs. Ignoring the SDs is not a concern because they are similar across the subjects. The paired t-test was preferred to a GEE or other model-based analysis that may not be reliable with so few subjects. One drawback of the paired t-test analysis was that it excluded case 5 who only had demyelinated lesions and no PPWM for paired comparison.

3.3 Results

3.3.1 Tissue Pathology

The cohort examined in this study included three male and three female patients, ranging from four to seventy-nine years of age. The patients' clinical data were not available and therefore the diagnosis of definite MS could not be fulfilled. Thus, all patients presented here had the diagnosis of clinically isolated syndrome (CIS), which is a single neurological episode suggestive of MS. However, all six biopsies showed pathological findings consistent with MS: confluent demyelinated lesions infiltrated by a sea of myelin-laden macrophages. Perivascular demyelination consistent with acute disseminated encephalomyelitis (ADEM), or astrocytic

damage, aquaporin-4 (AQP4) loss, granulocyte infiltration, myelin vacuolation and vascular fibrosis consistent with neuromyelitis optica (NMO) were not found. Only two of the six cases could be immunopatterned because they contained early active lesions. The other four cases contained late active lesions. The markers of oxidative injury in demyelinated lesions and PPWM were compared in this study.

3.3.2 Differential Distribution of Sulphur, Phosphate, And Iron in Demyelinated Lesions and Periplaque White Matter

XFI revealed that sulphur was decreased in demyelinated lesions in all six biopsies (Fig. 3.1A) when compared to PPWM (Fig. 3.1B). Sulphur was uniformly distributed in demyelinated lesions, but in Case 1, increased sulphur was present around blood vessels (Fig. 3.1A, *asterisks*) and co-localized with an area containing a high density of perivascular macrophages (Fig. 3.1G, I, K). Haemorrhagic areas contained the most sulphur in the PPWM (Fig. 3.1B, H, J, *arrows*).

Phosphorous was lost in the demyelinated lesions in all biopsies (Fig. 3.1C) but not in PPWM (Fig. 3.1D). Similar to the distribution of sulfur, higher phosphorous co-localized with perivascular macrophages in the demyelinated lesion (Fig. 3.1C, G, I, K, *arrows*). As opposed to sulfur, the haemorrhagic areas contained the lowest phosphorous in the PPWM (Fig. 3.1D, H, J, *arrows*).

The loss of both sulphur and phosphorous in the demyelinated lesions corresponded to the myelin loss, reflected by a loss of PLP immunoreactivity (Fig. 3.1G) and a lack of LFB-HE staining (Fig. 3.1I) compared to the PPWM (Fig. 3.1H, J).

The distribution of iron varied between biopsies. Iron distinctly localized to perivascular macrophages (Fig. 3.1E) and hemorrhages in lesions in two cases. Only two cases did not show a distinct difference in iron distribution between the demyelinated lesions and PPWM. The identity of macrophages was confirmed with CD68 immunohistochemistry (Fig. 3.1K). The iron in PPWM most likely corresponded to oligodendrocytes and myelin (Fig. 3.1F). CD68 immunohistochemistry showed a uniform distribution of microglia in the PPWM (Fig. 3.1L).

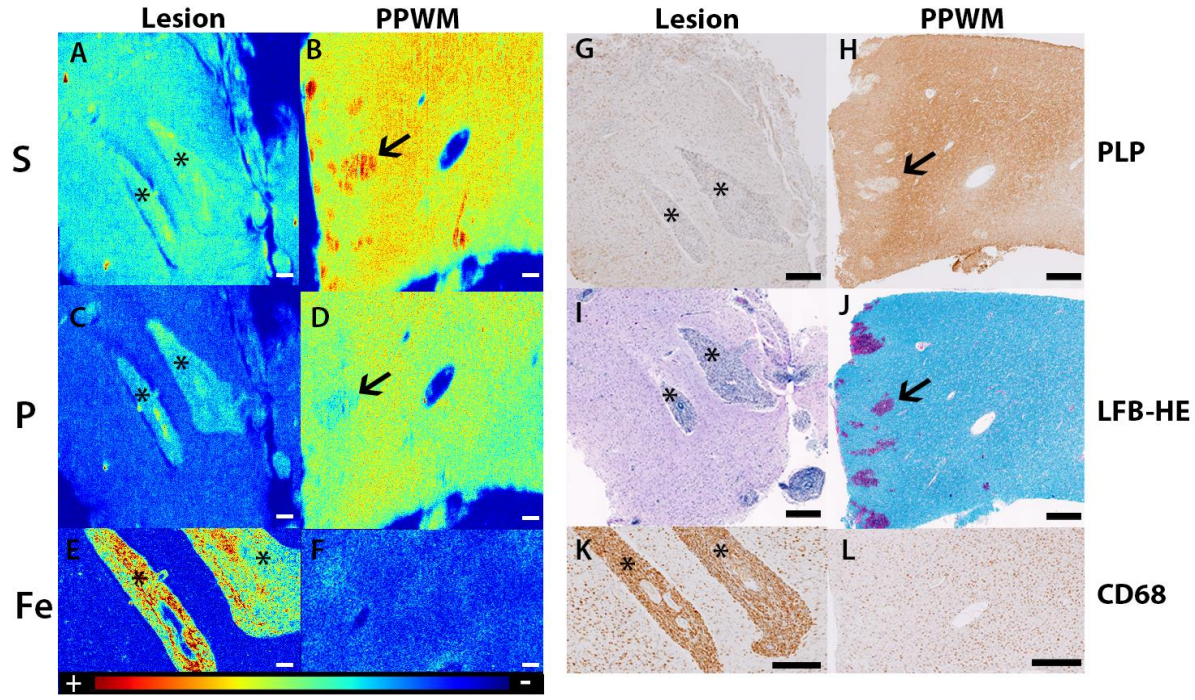

Figure 3.1 X-ray fluorescence imaging of an MS biopsy reveals loss of sulphur and phosphorous in demyelinated lesions, and accumulation of phosphorous and iron in perivascular macrophages. Sulphur (A) is lost in demyelinated lesions (XFI) and (B) is preserved in periplaque white matter (PPWM) where the highest sulphur concentrations correspond to hemorrhages (*arrow*) (XFI). (C) Phosphorous is lost in the demyelinated lesion, but accumulates in macrophages surrounding blood vessels (*asterisks)* (XFI). (D) Phosphorous is evenly distributed throughout the PPWM and lost at hemorrhage sites (*arrow*) (XFI). (E) Iron is lost in demyelinated lesions, but accumulates in perivascular macrophages (XFI). (F) Iron in PPWM has a patchy distribution (XFI). (G) Myelin loss is confirmed by absence of proteolipid protein immunoreactivity (PLP) while (H) myelin is preserved in the PPWM with visible hemorrhages (*arrow*) (PLP). (I) Luxol-fast blue/Hematoxylin & Eosin also shows complete loss of myelin in the lesion (LFB-HE). (J) Myelin appears blue in the PPWM and hemorrhages stain dark purple (*arrow*) (LFB-HE). (K) macrophages accumulate perivascularly, they also in the brain parenchyma (CD68). (L) Activated microglia are present in the PPWM (CD68). Intensity scale bar applies to all XFI images and represents the normalized total Kα fluorescence counts, proportional to total chemical element present with blue as lowest and red as highest. Scale bars: A-D) 100 µm; E & F) 60 µm; G- L) 1 mm.

3.3.3 Ferrihydrite is the Predominant Iron Species in Perivascular Macrophages

Because there was such a remarkable amount of iron seen in the perivascular macrophages in the demyelinated lesion of case 1 (Fig. 3.1E), chemically specific iron imaging was performed on this case alone to determine form of iron present macrophages. Interestingly, perivascular macrophages in the lesion contained mostly ferrihydrite (Fig. 3.2C). The amounts of iron-sulphur clusters (Fig. 3.2A) and ferrous iron (Fig. 3.2B) in the lesion were negligible. Similarly, the majority of iron in the PPWM was ferrihydrite (Fig. 3.2F), with very little amounts of iron-sulphur clusters (Fig. 3.2D) and ferrous iron (Fig. 3.2E) present.

Because ferrihydrite is the mineral core of ferritin, all six biopsies were stained immunohistochemically for heavy-chain ferritin (HF) and light-chain ferritin (LF). Myelin (Fig. 3.2G), perivascular macrophages (Fig. 3.2H), astrocytes and nuclei of some oligodendrocytes were immunoreactive for HF in the demyelinated lesions. In the PPWM, HF stained myelin and oligodendrocytes (Fig. 3.2I).

Myelin was immunonegative for LH in the lesions (Fig. 3.2J) and PPWM (Fig. 3.2L). In the demyelinated lesions macrophages (Fig. 3.2K) and reactive astrocytes were immunoreactive for LF, while in the PPWM, LF stained microglia (Fig. 3.2L).

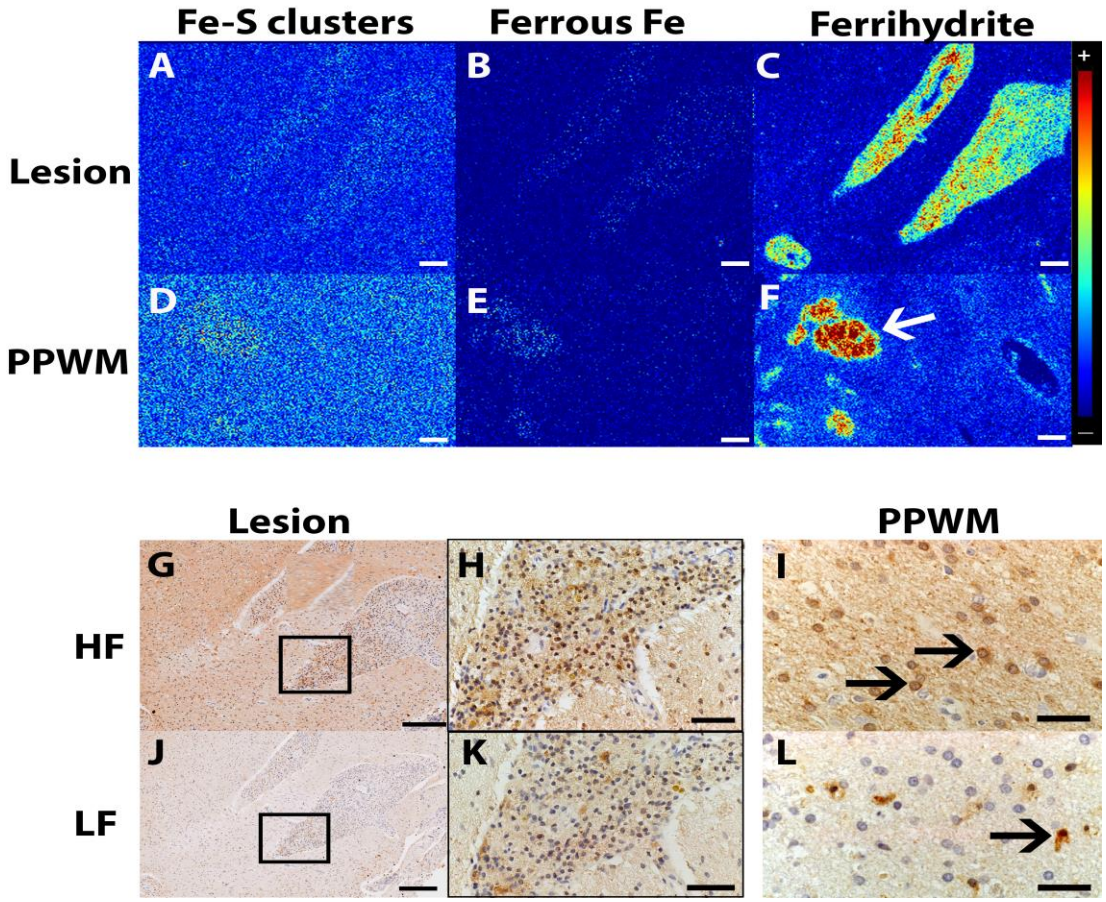

Figure 3.2 Chemically specific XFI shows most iron in demyelinated lesions and normal appearing white matter is stored as ferrihydrite. Chemically specific XFI shows the absence of (A) Fe-S clusters (XFI) and (B) ferrous iron (XFI) in the demyelinated lesion. (C) Most iron in the demyelinated lesion is ferrihydrite (XFI). Similarly, (D) iron-sulphur clusters (XFI) and (E) ferrous iron (XFI) are mostly absent in the periplaque white matter (PPWM), except for small amounts present in hemorrhages (F, *arrow*). (F) Most iron in the PPWM is present as ferrihydrite (XFI). Ferritin immunohistochemistry shows H-ferritin immunoreactivity on (G) myelin (HF) and in (H) perivascular macrophages (HF). (I) H-ferritin in PPWM is localized to oligodendrocytes (*arrows*). (J and K) Macrophages in the demyelinated lesions (LF) and (L) activated microglia in the PPWM (LF) are immunoreactive for L-ferritin. Intensity scale bar applies to the all XFI images and represents the normalized total Kα fluorescence counts, proportional to total metal present with blue as lowest and red as highest. Scale bars: A-F) 100 µm; H & K) 50 µm; I & L) 33.3 µm; G & J) 200 µm.

3.3.4 Lipid Oxidation Precedes Oxidation of Proteins

Several different areas within the lesion and PPWM were chosen for spectrum collection and the spectra shown in figure 3.4A represent an average of all collected spectra. The CH_2/CH_3 and CH_2/total lipid ratios can be used as indicators of lipid oxidation. Demyelinated lesions had lower CH_2/CH_3 ratio than PPWM (Fig. 3.4A), which was consistent across all biopsies (Fig. 3.5A). A reduced CH_2/CH_3 ratio likely indicates increased lipid oxidation and can be due to lipid acyl chain unsaturation occurring during lipid peroxidation. However, oxidation of proteins may lead to production of carbonyl groups on amino acid residues that also contribute to the changes seen in CH_3. Thus, using CH_2/total lipid ratios bypasses the use of CH_3 confirming the presence of lipid oxidation. Quantification of lipid oxidation using the two ratios of CH_2/CH_3 and CH_2/ total lipid is listed in Table 3.1.

There were also changes in the carbonyl ester (C=O) vibration at 1740 cm^{-1} that was mainly associated with the lipid ester. Lipid ester is an important functional group associated with myelin and demyelinated lesions had lower lipid ester than PPWM (Fig. 3.4A).

Protein conformational changes were indicated in the Amide I region (1700-1600 cm^{-1}), which mainly arise from C=O stretches from the protein backbone (Miller, Bourassa, & Smith, 2013). The shift in the position of the Amide I band and the appearance of a shoulder indicated altered protein secondary structure within the demyelinated lesion (Fig. 3.4A).

Further analysis of second-derivative spectra (Fig. 3.4B), to enhance peak deconvolution, revealed increased intensity at 1635-1620 cm^{-1} and decreased intensity at 1660-1650 cm^{-1}. These alterations are characteristic of increased beta sheets and decreased alpha-helix protein secondary structures in demyelinated lesions (Table 3.1). Increased beta sheets/protein aggregation was consistent across all biopsies (Fig. 3.5B).

There were changes in asymmetric phosphate (P-O) vibration at 1240 cm^{-1} with lower phosphate in demyelinated lesions compared to PPWM (Fig. 3.4A). Lower phosphate in demyelinated lesions was observed across all biopsies (Fig. 3.5C and Table 1).

While infrared imaging suggested a decrease in alpha helices in lesions versus the PPWM (Fig. 3.3A and B), this difference was not statistically significant ($p=0.13$) (Fig. 3.6). There also was no difference in the amount of total proteins between the lesions and PPWM ($p=0.3$) (Fig.

3.6). There was a trend for increased beta sheets in demyelinated lesions (p=0.07) compared to PPWM (Fig. 3.3C and D), and this increase reached statistical significance when beta sheets were normalized to either normal conformed proteins (p=0.03) or total proteins (p=0.05) (Fig. 3.6).

Total lipids were significantly decreased in demyelinated lesions (p=0.05, Fig. 3.3E) compared to PPWM (Fig. 3.3F) and oxidized lipids accumulated in demyelinated lesions (Fig. 3.3G) versus PPWM (Fig. 3.3H) (CH_2/CH_3 p=0.04 and CH_2/total lipid p=0.02). Notably, not many of the lipid-rich perivascular macrophages contained oxidized lipids (Fig. 3.3H).

There was significant phosphate loss in lesions (p=0.04, Fig. 3.3I) compared to PPWM (Fig. 3.3J).

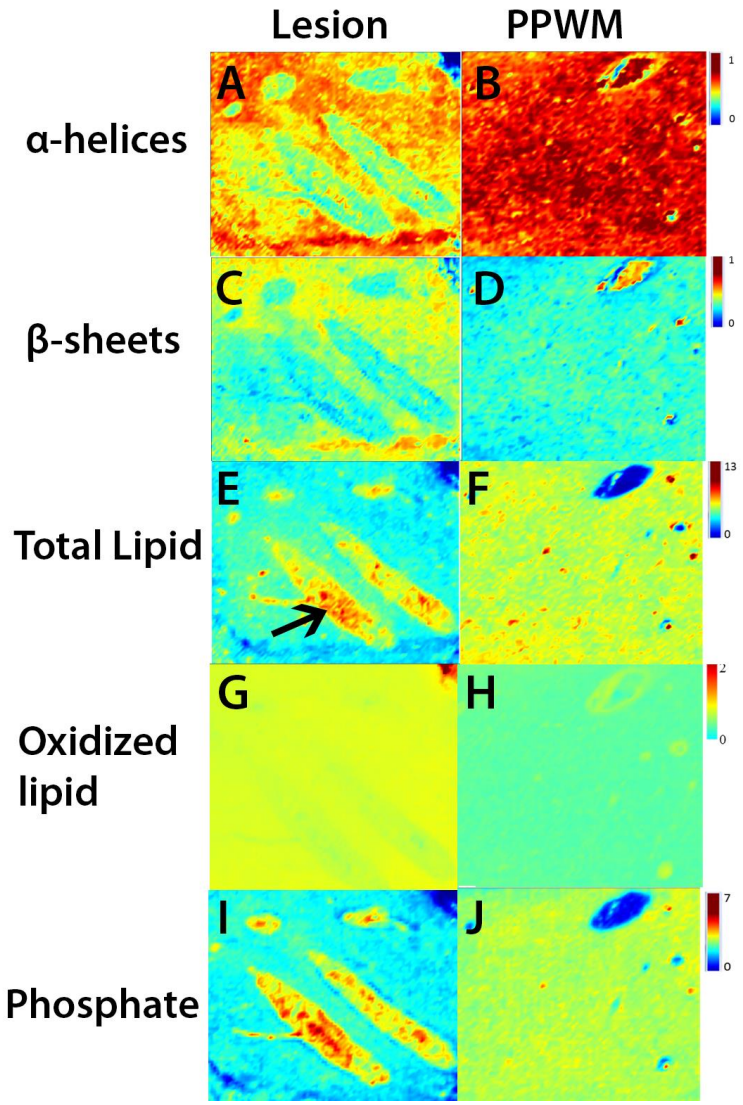

Figure 3.3 Infrared imaging of demyelinated lesion of an MS biopsy shows oxidation of proteins and lipids. Alpha helices, indicative of normal proteins, are decreased in demyelinated lesions (A), but not in periplaque white matter (PPWM) (B). Beta sheets, an indicator of proteins with abnormal conformation, are increased in demyelinated lesions (C) when compared to PPWM (D). Total lipids are lost in demyelinated lesions (E), but is not in the PPWM (F). Perivascular macrophages contain high amounts of lipids (E, *arrow*). Lipid oxidation is more prominent in demyelinated lesion (G) than in the PPWM (H). Phosphate is lost in the lesion where it accumulates in perivascular macrophages (I), but is preserved in the PPWM (J).

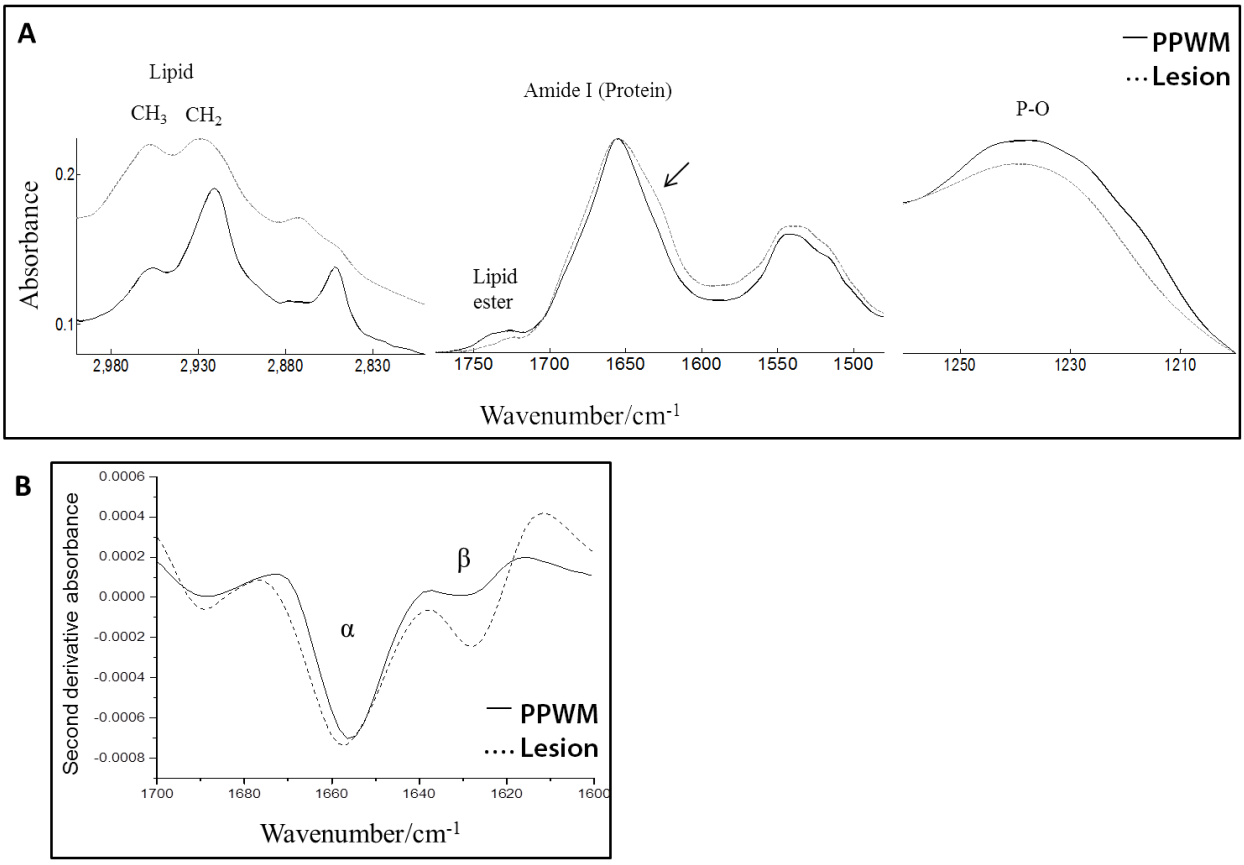

Figure 3.4 FTIR analysis shows increase lipid oxidation, accumulation of beta sheets and loss of phosphate in demyelinated lesions. The solid (dark grey) and dotted (light grey) lines indicate spectra collected from the periplaque white matter (PPWM) and lesions, respectively. The lipid spectra from the lesion and PPWM are staggered for better visualization of changes in the CH_2/CH_3 ratio. (A) The spectra show the differences between demyelinated lesions and the PPWM in the lipid, protein, and phosphate (P-O) regions. A reduction of the CH_2/CH_3 ratio indicates lipid acyl chain cleavage due to oxidation; a shift in the Amide I band indicates changes in protein secondary structure; decreased phosphate in demyelinated lesions. (B) The second derivative of the absorbance spectrum of Amide I (1700-1600 cm^{-1}) was performed to resolve the changes in alpha and beta protein secondary structures. Beta sheets (1628 cm^{-1}) accumulate in demyelinated lesions compared to the PPWM.

Table 3.1 Integrated intensities of molecular vibration bands of lipid, protein and phosphate.

Cases*	Total lipid	Oxidized lipid CH_2/CH_3	CH_2 / Total lipid	Total protein	β-sheets	α-helix	β-sheets / α-helix	β-sheets/ Total protein	Phosphate
1-M	11.765	2.902	0.685	24.809	3.308	6.124	0.540	0.133	0.775
	±0.211	±0.098	±0.065	±1.408	±0.154	±0.245	±0.075	±0.021	±0.101
1-D	6.117	1.443	0.537	24.355	3.842	5.337	0.719	0.158	0.390
	±0.128	±0.082	±0.041	±1.821	±0.165	±0.331	±0.068	±0.025	±0.085
2-D	6.402	1.804	0.582	24.975	3.550	5.761	0.616	0.142	0.355
	±0.154	±0.101	±0.076	±1.654	±0.162	±0.268	±0.056	±0.023	±0.099
2-M	10.172	3.011	0.665	24.294	3.458	5.769	0.599	0.143	0.678
	±0.232	±0.121	±0.081	±1.81	±0.173	±0.219	±0.045	±0.019	±0.089
3-M	11.086	2.85	0.658	24.356	3.175	5.837	0.544	0.130	0.680
	±0.258	±0.121	±0.074	±1.671	±0.147	±0.276	±0.043	±0.021	±0.097
3-D	9.513	2.41	0.508	23.943	3.475	5.839	0.595	0.145	0.601
	±0.215	±0.119	±0.101	±1.862	±0.171	±0.292	±0.049	±0.016	±0.087
4-M	7.343	2.29	0.608	24.169	3.390	5.732	0.519	0.140	0.460
	±0.165	±0.088	±0.062	±1.615	±0.132	±0.198	±0.042	±0.023	±0.078
4-D	7.090	2.013	0.59	22.763	3.345	5.367	0.623	0.147	0.423
	±0.154	±0.101	±0.058	±1.436	±0.148	±0.210	±0.039	±0.017	±0.067
5-Da	8.452	2.275	0.674	23.941	3.500	5.620	0.622	0.146	0.435
	±0.233	±0.109	±0.098	±1.722	±0.155	±0.188	±0.041	±0.022	±0.088
5-Db	7.465	2.17	0.613	23.665	3.563	5.517	0.646	0.150	0.329
	±0.198	±0.111	±0.114	±1.587	±0.169	±0.199	±0.055	±0.027	±0.099
6-D	7.113	2.454	0.539	23.912	3.403	5.637	0.604	0.142	0.581
	±0.208	±0.089	±0.103	±1.489	±0.179	±0.201	±0.051	±0.019	±0.092
6-M	8.830	2.813	0.616	24.264	3.077	5.871	0.524	0.127	0.741
	±0.199	±0.097	±0.118	±1.621	±0.187	±0.216	±0.049	±0.023	±0.084

Values presented with mean ± standard deviation. M = myelinated; D = demyelinated lesion; Da = first demyelinated region; Db= second demyelinated region

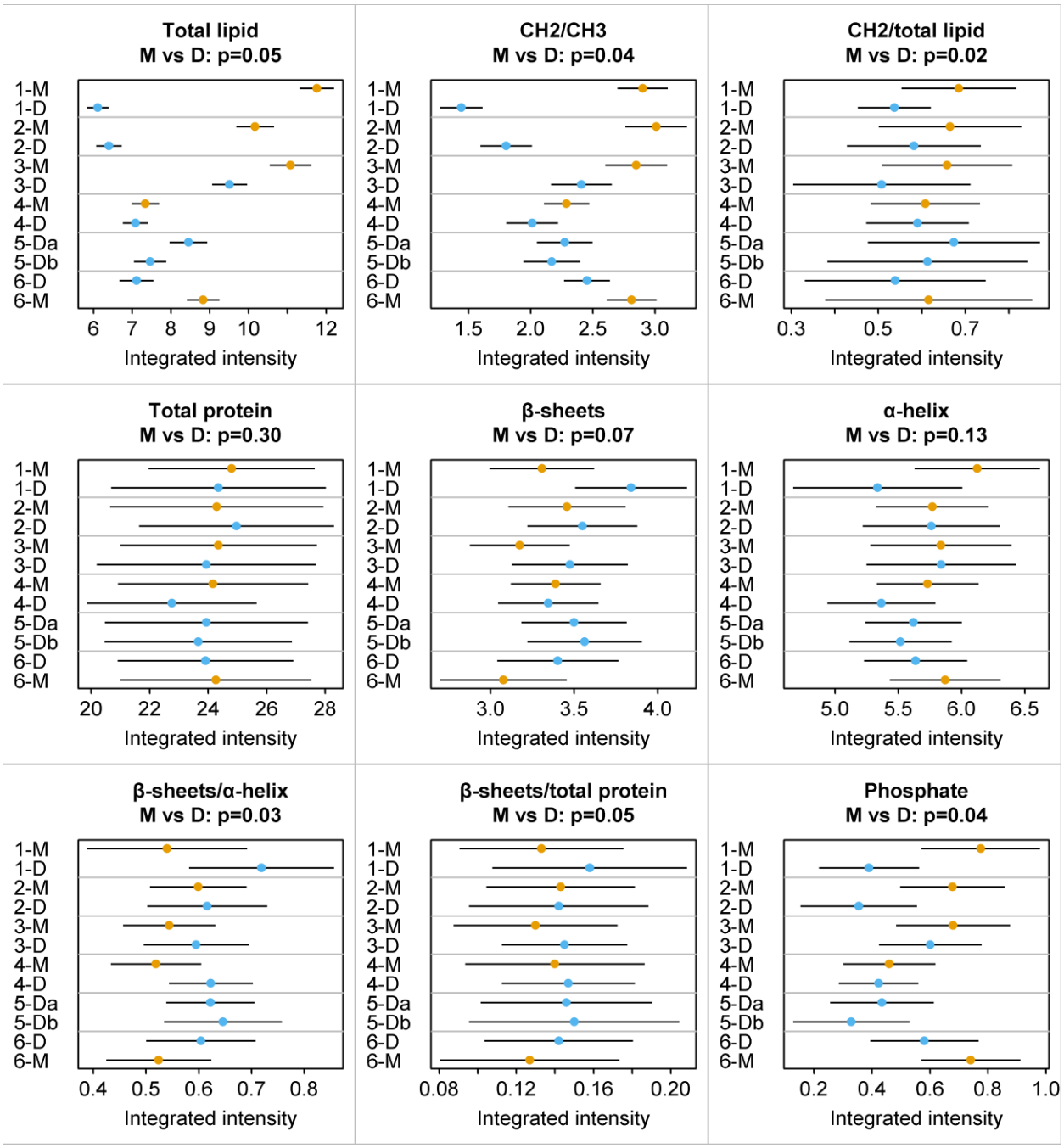

Figure 3.5 Graphical summary of oxidative damage markers in MS lesions compared to PPWM. Estimates with 2SD "error bars" or "precision bars" for myelinated (orange points) or demyelinated (blue points) lesions for each case. There is a significant increase in oxidized lipids and aggregated proteins, and a significant decrease in phosphate in MS lesions compared to the PPWM.

3.4 Discussion

A significant role has been proposed for oxidative injury in the process of demyelination and neurodegeneration in MS lesions (Lassmann, 2014a). This study clearly shows that oxidative injury of lipids and proteins is present in biopsied MS lesions and increased compared to the PPWM. Furthermore, I show that demyelinated lesions exhibit extensive lipid oxidation with comparatively low protein oxidation, indicating a possible temporal sequence where the oxidation of lipids precedes that of proteins. These findings also agree with previously published studies showing that oxidative injury is involved early in the pathogenesis of MS lesions (Haider et al., 2011).

Unsaturated fats, abundant in the CNS, are vulnerable to oxidative damage, and lipid peroxidation is a marker of oxidized lipids (Barnham, Masters, & Bush, 2004). Lipid peroxidation occurs when ROS attack carbon-carbon double bonds in lipids leading to formation of carbonyl groups (carbon atoms double bonded to oxygens) and the subsequent breakdown of long CH_2 chains into fragments (Ayala et al., 2014; LeVine & Wetzel, 1998). When the CH_2 chains are broken, a hydrogen is picked up by the fragments resulting in the creation of CH_3. Thus, an increase in CH_3 and a decrease in CH_2 is indicative of oxidized lipids. Oxidative damage in actively demyelinating MS lesions has been previously reported through the use of immunohistochemistry to detect the oxidative damage markers, 4-HNE and nitrotyrosine, indicative of damage to lipids and proteins, respectively. Foamy macrophages and hypertrophic astrocytes in actively demyelinating lesions contain high amounts of these oxidative markers. Using FTIR, my study confirms that biopsied active MS lesions contain significantly higher levels of oxidized lipids than PPWM. However, oxidized lipids do not co-localize with myelin-laden macrophages, but they are dispersed throughout the demyelinated lesion, possibly in reactive astrocytes or oligodendrocytes. A more recent study has found oxidized lipids primarily in oligodendrocytes and myelin within active MS lesions (Lassmann, 2014a). Oligodendrocytes are more vulnerable to oxidative damage compared to other glial cells due to their low levels of antioxidant enzymes, rendering them less efficient at responding to oxidative injury (Juurlink, Thorburne, & Hertz, 1998; van Horssen et al., 2008). Macrophages contain notably high levels of antioxidants (van Horssen et al., 2008) and are more resistant to oxidative damage. An *in vitro* study has shown that ingestion of human myelin by macrophages induces the expression of anti-inflammatory molecules characteristic for the M2-phenotype (Boven et al., 2006). Another study has found that myelin-laden macrophages in

demyelinated lesions express less p22phox and gp91phox, both of which are parts of the NADPH oxidase 2 (Nox2) complex (Fischer et al., 2012), and the deletion of gp91phox helps protect the animals from getting EAE (Li, Vana, Ribeiro, & Zhang, 2011). Thus, I believe that myelin-laden macrophages may serve a protective role in oxidative stress and also are important in resolving inflammation in MS lesions.

Lipid-rich areas have a prominent ester carbonyl band representing lipid esters (Caine et al., 2012). In the present study, MS lesions contained less lipid ester than PPWM, most likely due to the loss of myelin in the demyelinated lesions. XFI showed loss in sulphur that is likely also a reflection of demyelination since the sulphur-containing sulfatides are abundant constituents of myelin (Stuber et al., 2014).

To function normally, proteins need to fold into three-dimensional conformations. Partially folded or unfolded polypeptide chains are unstable and can aggregate into insoluble complexes (Cooper, 2000). FTIR is sensitive to protein secondary structures (Miller et al., 2013) and can be used as a unique fingerprinting tool to determine the relative protein secondary structure content or to determine alterations in protein secondary structure. The hydrogen bonding influences vibrational frequency and the variation in the polypeptide hydrogen bonding environment that is associated with different protein secondary structures is reflected in the position and intensity of the amide I band observed in FTIR spectra. I found a shift in the amide I band in demyelinated lesions indicating a change in the conformation of proteins. Analysis of the secondary structures showed that demyelinated lesions contained less normally folded proteins and significantly more aggregated proteins than PPWM. Interestingly normally folded proteins were relatively preserved compared to lipids and oxidized lipids in demyelinated lesions. This suggests that there is a temporal relationship in which oxidation of lipids precedes oxidation of proteins in MS lesion formation.

Protein oxidation can occur indirectly in a secondary protein carbonylation reaction, in which the end products of lipid peroxidation, such as 4-HNE, modify proteins and their function (Mirzaei & Regnier, 2008; Suzuki, Carini, & Butterfield, 2010). Protein oxidation leads to non-specific protein to protein interactions creating aggregates that compromise cell viability (Mirzaei & Regnier, 2008). Carbonylation is a type of protein oxidation that is often used as a marker of oxidative stress (Suzuki et al., 2010). Aggregated proteins can also result from primary protein

carbonylation reactions, which is direct oxidative attack resulting in the addition of carbonyl groups on amino acids such as proline, arginine, lysine, and threonine (Crichton, Dexter, & Ward, 2011; Fritz & Petersen, 2011). The aggregated proteins found in MS lesions may form similarly to amyloid plaques observed in Alzheimer's disease. Amyloid plaques are found in diseased tissues and have high β-sheet structure (Barnham et al., 2004). The present study showed an accumulation of β-sheets in demyelinated lesions compared to the PPWM suggesting the presence of protein oxidation and possible shared mechanism of damage between MS and some neurodegenerative disorders.

A few demyelinated lesions in this study were infiltrated with myelin-laden macrophages containing iron. It has been suggested that iron is liberated when the oligodendrocytes and myelin are destroyed in MS and taken up by microglia and macrophages (Hametner et al., 2013). In the one case where iron was chemically speciated, ferrihydrite, the mineral core of the iron storage protein ferritin, was the predominant iron species present in macrophages. Macrophages can alter expressions of proteins involved in iron metabolism to sequester iron, rendering it unavailable for pathways or pathogens that depend on iron (Gammella et al., 2014). This suggests that macrophages may play a protective role and attenuate tissue damage by sequestering free iron in demyelinated lesions, and argues against iron-caused oxidative damage in the earliest MS disease stages.

The reduced amount of phosphate and phosphorous found in the demyelinated lesions is likely due to demyelination and the subsequent loss of phospholipids. Cellular membranes are particularly vulnerable to oxidative damage because of the high concentrations of unsaturated fatty acids (Mukwevho et al., 2014). Active MS lesions express high levels of glutaminase (Carvalho et al., 2014), which is activated by inorganic phosphate (Bellocchio et al., 1998). Macrophages ingesting myelin and phosphatidylserine, a myelin phospholipid, have decreased nitric monoxide (NO) secretion that may slow disease progression (Bogie et al., 2013).

There is increasing evidence that oxidative stress plays a significant role in the pathogenesis of early MS, and it has become increasingly important to elucidate the mechanisms and characteristics of oxidative injury in human MS tissues. The oxidative damage in early MS does not seem to be driven by iron accumulation, and this again argues against the use of iron chelators in the treatment of early MS. However, the important role of oxidative injury of myelin

and oligodendrocytes plays in the earliest disease phases may open new therapeutic avenues for using antioxidants in the treatment of at least a subset of patients with RRMS.

Chapter 4 General Conclusions and Future Directions

Multiple sclerosis (MS) is the most common neurological disease of young adults for which there is no cure, but there are treatments available that can offer some degree of control over the inflammatory process reducing the frequency and severity of attacks (MS International Federation, 2015). Research suggests that relapsing-remitting MS benefits from early therapeutic interventions and this requires prompt and accurate diagnosis at the earliest stages of the disease (Katz Sand, 2015). It is becoming clear that the pathogenesis of MS is heterogeneous and more complex than previously thought. The presence of pathological heterogeneity between MS patients suggests that the mechanism of tissue injury and the mechanism of demyelination is distinctly different in different patient subgroups (Lucchinetti et al., 2000). None of the currently available therapeutics are effective for all MS patients and the reason behind this may be the heterogeneity of disease. It has been shown that different immunopatterns respond differently to various treatments: immunopattern II, but not immunopattern III, patients respond to plasmapheresis for treatment of steroid unresponsive MS relapses (Keegan et al., 2005). Thus, it is important to develop non-invasive methods to distinguish between the different immunopatterns in living patients. To accomplish this, it is crucial to identify reliable biomarkers for use in, for example, MRI. In my thesis, I used a multimodal approach with X-ray fluorescence imaging (XFI), Fourier-transform infrared spectroscopy (FTIR), and routine histology and immunohistochemistry to identify such potential MS biomarkers.

The content and distribution of iron within early active MS lesions is a promising biomarker that may be able to distinguish between immunopatterns. XFI is a novel tool that has not been previously used in a systematic way to study human MS brain tissues. While the first study has determined that there is a differential iron content and distribution between immunopattern II and III active lesions, additional studies are required to validate my findings *in vivo* using MRI. Several MRI techniques have been proposed to be sensitive to iron (Bagnato et al., 2011; Mehta et al., 2013; Zheng et al., 2013) and MRI is already used for studies of iron deposition in brains of living patients (Ropele et al., 2011). Therefore, these MRI modalities will have to be validated by XFI (Hopp et al., 2010; Zheng et al., 2013) and may be adapted for the identification of MS immunopatterns.

Immunopattern heterogeneity is characteristic for white matter lesions of early relapsing disease. The presence of early active MS lesions is a prerequisite for immunopattern classification, and this becomes problematic for patients with lesions that have evolved to a different demyelinating stage, for example late active or chronic lesions. Heterogeneous immunopatterns may ultimately converge into a uniform homogeneous pattern that contributes to MS progression in the absence of ongoing relapses. While immunopathological immunopatterns are no longer distinguishable in chronic MS, the iron signature that differentiates immunopattern II from immunopattern III MS may still be present. Future studies using late active or inactive lesions from patients with known immunopatterns will have to establish whether the iron accumulation that characterizes MS immunopatterns is still present past the early active lesion stage and can still differentiate between patients with immunopattern II and immunopattern III MS during the chronic disease phase.

Oxidative stress promotes demyelination and neurodegeneration in early MS (Lassmann, 2014b) and oxidized DNA, lipids, and protein are often found in active MS lesions (van Horssen et al., 2008). It has been proposed that oxidative damage in MS is driven by iron accumulation, but I show here that in early MS, demyelinated lesions are devoid of iron, a finding inconsistent with iron-driven oxidative tissue damage. Using FTIR imaging and XFI, I propose a list of potential biomarkers for early lesions: increased oxidized lipids and aggregated proteins, and lower amounts of iron, sulfur, phosphorus and phosphate. Future studies will have to establish if these markers can be identified *in vivo* using MRI, MR spectroscopy and/or other imaging modalities. Future studies will also have to establish if these oxidative biomarkers, in addition to iron, correlate with various immunopatterns. The identification of such *in vivo* biomarkers for early MS lesions and immunopatterns will allow the immunophenotyping of MS patients without the need of biopsy, an invasive and dangerous procedure. Furthermore, it will allow the stratification of MS patients and will have potentially significant therapeutic implications, as individualized therapeutic approaches to treat the early stages of the disease may need to be considered.

Chapter 5 References

Aboul-Enein, F., Rauschka, H., Kornek, B., Stadelmann, C., Stefferl, A., Bruck, W., . . . Lassmann, H. (2003). Preferential loss of myelin-associated glycoprotein reflects hypoxia-like white matter damage in stroke and inflammatory brain diseases. *J Neuropathol Exp Neurol, 62*(1), 25-33.

Alkhateeb, A. A., & Connor, J. R. (2010). Nuclear ferritin: A new role for ferritin in cell biology. *Biochim Biophys Acta, 1800*(8), 793-797. doi: 10.1016/j.bbagen.2010.03.017

Arosio, P., Carmona, F., Gozzelino, R., Maccarinelli, F., & Poli, M. (2015). The importance of eukaryotic ferritins in iron handling and cytoprotection. *Biochem J, 472*(1), 1-15. doi: 10.1042/BJ20150787

Asano, T., Koike, M., Sakata, S., Takeda, Y., Nakagawa, T., Hatano, T., . . . Iwai, K. (2015). Possible involvement of iron-induced oxidative insults in neurodegeneration. *Neurosci Lett, 588*, 29-35. doi: 10.1016/j.neulet.2014.12.052

Ayala, A., Munoz, M. F., & Arguelles, S. (2014). Lipid peroxidation: production, metabolism, and signaling mechanisms of malondialdehyde and 4-hydroxy-2-nonenal. *Oxid Med Cell Longev, 2014*, 360438. doi: 10.1155/2014/360438

Bagnato, F., Hametner, S., Yao, B., van Gelderen, P., Merkle, H., Cantor, F. K., . . . Duyn, J. H. (2011). Tracking iron in multiple sclerosis: a combined imaging and histopathological study at 7 Tesla. *Brain, 134*(Pt 12), 3602-3615. doi: 10.1093/brain/awr278

Barnett, M. H., Parratt, J. D., Cho, E. S., & Prineas, J. W. (2009). Immunoglobulins and complement in postmortem multiple sclerosis tissue. *Ann Neurol, 65*(1), 32-46. doi: 10.1002/ana.21524

Barnett, S. C., & Linington, C. (2013). Myelination: do astrocytes play a role? *Neuroscientist, 19*(5), 442-450. doi: 10.1177/1073858412465655

Barnham, K. J., Masters, C. L., & Bush, A. I. (2004). Neurodegenerative diseases and oxidative stress. *Nat Rev Drug Discov, 3*(3), 205-214. doi: 10.1038/nrd1330

Bedard, K., & Krause, K. H. (2007). The NOX family of ROS-generating NADPH oxidases: physiology and pathophysiology. *Physiol Rev, 87*(1), 245-313. doi: 10.1152/physrev.00044.2005

Bellocchio, E. E., Hu, H., Pohorille, A., Chan, J., Pickel, V. M., & Edwards, R. H. (1998). The localization of the brain-specific inorganic phosphate transporter suggests a specific presynaptic role in glutamatergic transmission. *J Neurosci, 18*(21), 8648-8659.

Berlett, B. S., & Stadtman, E. R. (1997). Protein oxidation in aging, disease, and oxidative stress. *J Biol Chem, 272*(33), 20313-20316.

Bitsch, A., & Bruck, W. (2002). Differentiation of multiple sclerosis subtypes: implications for treatment. *CNS Drugs, 16*(6), 405-418.

Blumenfeld, H. (2010). *Neuroanatomy through clinical cases* (2nd ed.). Sunderland, MA: Sinauer Associates, Inc. Publishers.

Bogie, J. F., Jorissen, W., Mailleux, J., Nijland, P. G., Zelcer, N., Vanmierlo, T., . . . Hendriks, J. J. (2013). Myelin alters the inflammatory phenotype of macrophages by activating PPARs. *Acta Neuropathol Commun, 1*, 43. doi: 10.1186/2051-5960-1-43

Bove, R., & Chitnis, T. (2014). The role of gender and sex hormones in determining the onset and outcome of multiple sclerosis. *Mult Scler, 20*(5), 520-526. doi: 10.1177/1352458513519181

Boven, L. A., Van Meurs, M., Van Zwam, M., Wierenga-Wolf, A., Hintzen, R. Q., Boot, R. G., . . . Laman, J. D. (2006). Myelin-laden macrophages are anti-inflammatory, consistent with foam cells in multiple sclerosis. *Brain, 129*(Pt 2), 517-526. doi: 10.1093/brain/awh707

Bruck, W., Porada, P., Poser, S., Rieckmann, P., Hanefeld, F., Kretzschmar, H. A., & Lassmann, H. (1995). Monocyte/macrophage differentiation in early multiple sclerosis lesions. *Ann Neurol, 38*(5), 788-796. doi: 10.1002/ana.410380514

Bruck, W., Sommermeier, N., Bergmann, M., Zettl, U., Goebel, H. H., Kretzschmar, H. A., & Lassmann, H. (1996). Macrophages in multiple sclerosis. *Immunobiology, 195*(4-5), 588-600. doi: 10.1016/S0171-2985(96)80024-6

Bush, V. J., Moyer, T. P., Batts, K. P., & Parisi, J. E. (1995). Essential and toxic element concentrations in fresh and formalin-fixed human autopsy tissues. *Clin Chem, 41*(2), 284-294.

Caine, S., Heraud, P., Tobin, M. J., McNaughton, D., & Bernard, C. C. (2012). The application of Fourier transform infrared microspectroscopy for the study of diseased central nervous system tissue. *Neuroimage, 59*(4), 3624-3640. doi: 10.1016/j.neuroimage.2011.11.033

Cairo, G., Recalcati, S., Mantovani, A., & Locati, M. (2011). Iron trafficking and metabolism in macrophages: contribution to the polarized phenotype. *Trends Immunol, 32*(6), 241-247. doi: 10.1016/j.it.2011.03.007

Calabrese, M., & Gallo, P. (2009). Magnetic resonance evidence of cortical onset of multiple sclerosis. *Mult Scler, 15*(8), 933-941. doi: 10.1177/1352458509106510

Canadian Light Source, I. (2012). What is a Synchrotron. from http://www.lightsource.ca/education/whatis.php

Carvalho, A. N., Lim, J. L., Nijland, P. G., Witte, M. E., & Van Horssen, J. (2014). Glutathione in multiple sclerosis: More than just an antioxidant? *Mult Scler, 20*(11), 1425-1431. doi: 10.1177/1352458514533400

Chalmers, J. M. (2011). Mid-infrared Spectroscopy: The Basics. In D. Moss (Ed.), *Biomedical Applications of Synchrotron Infrared Microspectroscopy* (pp. 29-66). Cambridge, UK: Royal Society of Chemistry.

Chasteen, N. D., & Harrison, P. M. (1999). Mineralization in ferritin: an efficient means of iron storage. *J Struct Biol, 126*(3), 182-194. doi: 10.1006/jsbi.1999.4118

Choo, L. P., Jackson, M., Halliday, W. C., & Mantsch, H. H. (1993). Infrared spectroscopic characterisation of multiple sclerosis plaques in the human central nervous system. *Biochim Biophys Acta, 1182*(3), 333-337.

Chua-anusorn, W., Webb, J., Macey, D. J., Pootrakul, P., & St Pierre, T. G. (1997). The effect of histological processing on the form of iron in iron-loaded human tissues. *Biochim Biophys Acta, 1360*(3), 255-261.

Connor, J. R., & Menzies, S. L. (1996). Relationship of iron to oligodendrocytes and myelination. *Glia, 17*(2), 83-93. doi: 10.1002/(SICI)1098-1136(199606)17:2<83::AID-GLIA1>3.0.CO;2-7

Connor, J. R., Ponnuru, P., Wang, X. S., Patton, S. M., Allen, R. P., & Earley, C. J. (2011). Profile of altered brain iron acquisition in restless legs syndrome. *Brain, 134*(Pt 4), 959-968. doi: 10.1093/brain/awr012

Cooper, G. M. (2000). Protein Folding and ProcessingThe Cell: A Molecular Approach (2 ed.). Sunderland, MA: Sinauer Associates. Retrieved from http://www.ncbi.nlm.nih.gov/books/NBK9843/.

Corna, G., Campana, L., Pignatti, E., Castiglioni, A., Tagliafico, E., Bosurgi, L., . . . Rovere-Querini, P. (2010). Polarization dictates iron handling by inflammatory and alternatively activated macrophages. *Haematologica, 95*(11), 1814-1822. doi: 10.3324/haematol.2010.023879

Craelius, W., Migdal, M. W., Luessenhop, C. P., Sugar, A., & Mihalakis, I. (1982). Iron deposits surrounding multiple sclerosis plaques. *Arch Pathol Lab Med, 106*(8), 397-399.

Creange, A., Lefaucheur, J. P., Balleyguier, M. O., & Galacteros, F. (2013). Iron depletion induced by bloodletting and followed by rhEPO administration as a therapeutic strategy in progressive multiple sclerosis: a pilot, open-label study with neurophysiological measurements. *Neurophysiol Clin, 43*(5-6), 303-312. doi: 10.1016/j.neucli.2013.09.004

Crichton, R. R. (2009). *Iron Metabolism - From Molecular Mechanisms to Clinical Consequences* (3rd ed.). West Sussex, UK: John Wiley & Sons Ltd.

Crichton, R. R., Dexter, D. T., & Ward, R. J. (2011). Brain iron metabolism and its perturbation in neurological diseases. *J Neural Transm, 118*(3), 301-314. doi: 10.1007/s00702-010-0470-z

Cross, A. H., & Piccio, L. (2014). Immunopathogenesis of Multiple Sclerosis. In L. M. Samkoff & A. D. Goodman (Eds.), *Multiple Sclerosis and CNS Inflammatory Disorders* (pp. 10-17). West Sussex, UK: John Wiley & Sons, Ltd.

De Groot, C. J., Bergers, E., Kamphorst, W., Ravid, R., Polman, C. H., Barkhof, F., & van der Valk, P. (2001). Post-mortem MRI-guided sampling of multiple sclerosis brain lesions: increased yield of active demyelinating and (p)reactive lesions. *Brain, 124*(Pt 8), 1635-1645.

Dimitrov, J. D., Roumenina, L. T., Doltchinkova, V. R., & Vassilev, T. L. (2007). Iron ions and haeme modulate the binding properties of complement subcomponent C1q and of immunoglobulins. *Scand J Immunol, 65*(3), 230-239. doi: 10.1111/j.1365-3083.2006.01893.x

Farina, C., Aloisi, F., & Meinl, E. (2007). Astrocytes are active players in cerebral innate immunity. *Trends Immunol, 28*(3), 138-145. doi: 10.1016/j.it.2007.01.005

Filippi, M., Rocca, M. A., Barkhof, F., Bruck, W., Chen, J. T., Comi, G., . . . Lassmann, H. (2012). Association between pathological and MRI findings in multiple sclerosis. *Lancet Neurol, 11*(4), 349-360. doi: 10.1016/S1474-4422(12)70003-0

Fischer, M. T., Sharma, R., Lim, J. L., Haider, L., Frischer, J. M., Drexhage, J., . . . Lassmann, H. (2012). NADPH oxidase expression in active multiple sclerosis lesions in relation to oxidative tissue damage and mitochondrial injury. *Brain, 135*(Pt 3), 886-899. doi: 10.1093/brain/aws012

Friedman, A., Arosio, P., Finazzi, D., Koziorowski, D., & Galazka-Friedman, J. (2011). Ferritin as an important player in neurodegeneration. *Parkinsonism Relat Disord, 17*(6), 423-430. doi: 10.1016/j.parkreldis.2011.03.016

Frischer, J. M., Weigand, S. D., Guo, Y., Kale, N., Parisi, J. E., Pirko, I., . . . Lucchinetti, C. F. (2015). Clinical and pathological insights into the dynamic nature of the white matter multiple sclerosis plaque. *Ann Neurol, 78*(5), 710-721. doi: 10.1002/ana.24497

Fritz, K. S., & Petersen, D. R. (2011). Exploring the biology of lipid peroxidation-derived protein carbonylation. *Chem Res Toxicol, 24*(9), 1411-1419. doi: 10.1021/tx200169n

Fuchs, P., Perez-Pinzon, M. A., & Dave, K. R. (2014). Cerebral Ischemia in Diabetics and Oxidative Stress. In V. R. Preedy (Ed.), *Diabetes: Oxidative Stress and Antioxidants* (pp. 15-23). San Diego, CA, USA: Elsevier.

Gammella, E., Buratti, P., Cairo, G., & Recalcati, S. (2014). Macrophages: central regulators of iron balance. *Metallomics, 6*(8), 1336-1345. doi: 10.1039/c4mt00104d

Gartner, L. P., & Hiatt, J. L. (2007). *Color textbook of histology* (3rd ed.). Philadelphia, PA: Saunders Elsevier.

Goormaghtigh, E., Ruysschaert, J. M., & Raussens, V. (2006). Evaluation of the information content in infrared spectra for protein secondary structure determination. *Biophys J, 90*(8), 2946-2957. doi: 10.1529/biophysj.105.072017

Haacke, E. M., Makki, M., Ge, Y., Maheshwari, M., Sehgal, V., Hu, J., . . . Grossman, R. I. (2009). Characterizing iron deposition in multiple sclerosis lesions using susceptibility weighted imaging. *J Magn Reson Imaging, 29*(3), 537-544. doi: 10.1002/jmri.21676

Hackett, M. J., McQuillan, J. A., El-Assaad, F., Aitken, J. B., Levina, A., Cohen, D. D., . . . Lay, P. A. (2011). Chemical alterations to murine brain tissue induced by formalin fixation: implications for biospectroscopic imaging and mapping studies of disease pathogenesis. *Analyst, 136*(14), 2941-2952. doi: 10.1039/c0an00269k

Hader, W. J., & Yee, I. M. (2007). Incidence and prevalence of multiple sclerosis in Saskatoon, Saskatchewan. *Neurology, 69*(12), 1224-1229. doi: 10.1212/01.wnl.0000276991.13764.77

Haider, L. (2015). Inflammation, Iron, Energy Failure, and Oxidative Stress in the Pathogenesis of Multiple Sclerosis. *Oxid Med Cell Longev, 2015*, 725370. doi: 10.1155/2015/725370

Haider, L., Fischer, M. T., Frischer, J. M., Bauer, J., Hoftberger, R., Botond, G., . . . Lassmann, H. (2011). Oxidative damage in multiple sclerosis lesions. *Brain, 134*(Pt 7), 1914-1924. doi: 10.1093/brain/awr128

Hametner, S., Wimmer, I., Haider, L., Pfeifenbring, S., Bruck, W., & Lassmann, H. (2013). Iron and neurodegeneration in the multiple sclerosis brain. *Ann Neurol, 74*(6), 848-861. doi: 10.1002/ana.23974

Higgins, G. C., Beart, P. M., Shin, Y. S., Chen, M. J., Cheung, N. S., & Nagley, P. (2010). Oxidative stress: emerging mitochondrial and cellular themes and variations in neuronal injury. *J Alzheimers Dis, 20 Suppl 2*, S453-473. doi: 10.3233/JAD-2010-100321

Hopp, K., Popescu, B. F., McCrea, R. P., Harder, S. L., Robinson, C. A., Haacke, M. E., . . . Nichol, H. (2010). Brain iron detected by SWI high pass filtered phase calibrated with synchrotron X-ray fluorescence. *J Magn Reson Imaging, 31*(6), 1346-1354. doi: 10.1002/jmri.22201

Hulet, S. W., Powers, S., & Connor, J. R. (1999). Distribution of transferrin and ferritin binding in normal and multiple sclerotic human brains. *J Neurol Sci, 165*(1), 48-55.

Ingram, G., Hakobyan, S., Robertson, N. P., & Morgan, B. P. (2009). Complement in multiple sclerosis: its role in disease and potential as a biomarker. *Clin Exp Immunol, 155*(2), 128-139. doi: 10.1111/j.1365-2249.2008.03830.x

Juurlink, B. H., Thorburne, S. K., & Hertz, L. (1998). Peroxide-scavenging deficit underlies oligodendrocyte susceptibility to oxidative stress. *Glia, 22*(4), 371-378.

Katsumoto, A., Lu, H., Miranda, A. S., & Ransohoff, R. M. (2014). Ontogeny and functions of central nervous system macrophages. *J Immunol, 193*(6), 2615-2621. doi: 10.4049/jimmunol.1400716

Katz Sand, I. (2015). Classification, diagnosis, and differential diagnosis of multiple sclerosis. *Curr Opin Neurol, 28*(3), 193-205. doi: 10.1097/WCO.0000000000000206

Keegan, M., Konig, F., McClelland, R., Bruck, W., Morales, Y., Bitsch, A., . . . Lucchinetti, C. F. (2005). Relation between humoral pathological changes in multiple sclerosis and response to therapeutic plasma exchange. *Lancet, 366*(9485), 579-582. doi: 10.1016/S0140-6736(05)67102-4

Kim, K.-J. (2009). Characteristics of Synchrotron Radiation. In A. C. Thompson (Ed.), *X-ray Data Booklet* (3rd ed., pp. 1-16). Berkeley, California: Lawrence Berkeley National Laboratory.

Kluver, H., & Barrera, E. (1953). A method for the combined staining of cells and fibers in the nervous system. *J Neuropathol Exp Neurol, 12*(4), 400-403.

Kuhlmann, T., Lassmann, H., & Bruck, W. (2008). Diagnosis of inflammatory demyelination in biopsy specimens: a practical approach. *Acta Neuropathol, 115*(3), 275-287. doi: 10.1007/s00401-007-0320-8

Lassmann, H. (2014a). Mechanisms of white matter damage in multiple sclerosis. *Glia, 62*(11), 1816-1830. doi: 10.1002/glia.22597

Lassmann, H. (2014b). Multiple sclerosis: lessons from molecular neuropathology. *Exp Neurol, 262 Pt A*, 2-7. doi: 10.1016/j.expneurol.2013.12.003

Lassmann, H., Bruck, W., & Lucchinetti, C. F. (2007). The immunopathology of multiple sclerosis: an overview. *Brain Pathol, 17*(2), 210-218. doi: 10.1111/j.1750-3639.2007.00064.x

Leitner, D. F., & Connor, J. R. (2012). Functional roles of transferrin in the brain. *Biochim Biophys Acta, 1820*(3), 393-402. doi: 10.1016/j.bbagen.2011.10.016

LeVine, S. M. (1997). Iron deposits in multiple sclerosis and Alzheimer's disease brains. *Brain Res, 760*(1-2), 298-303.

LeVine, S. M., Bilgen, M., & Lynch, S. G. (2013). Iron accumulation in multiple sclerosis: an early pathogenic event. *Expert Rev Neurother, 13*(3), 247-250. doi: 10.1586/ern.13.14

LeVine, S. M., Lynch, S. G., Ou, C. N., Wulser, M. J., Tam, E., & Boo, N. (1999). Ferritin, transferrin and iron concentrations in the cerebrospinal fluid of multiple sclerosis patients. *Brain Res, 821*(2), 511-515.

LeVine, S. M., & Wetzel, D. L. (1998). Chemical analysis of multiple sclerosis lesions by FT-IR microspectroscopy. *Free Radic Biol Med, 25*(1), 33-41.

Li, S., Vana, A. C., Ribeiro, R., & Zhang, Y. (2011). Distinct role of nitric oxide and peroxynitrite in mediating oligodendrocyte toxicity in culture and in experimental autoimmune encephalomyelitis. *Neuroscience, 184*, 107-119. doi: 10.1016/j.neuroscience.2011.04.007

Link, H., & Huang, Y. M. (2006). Oligoclonal bands in multiple sclerosis cerebrospinal fluid: an update on methodology and clinical usefulness. *J Neuroimmunol, 180*(1-2), 17-28. doi: 10.1016/j.jneuroim.2006.07.006

London, A., Cohen, M., & Schwartz, M. (2013). Microglia and monocyte-derived macrophages: functionally distinct populations that act in concert in CNS plasticity and repair. *Front Cell Neurosci, 7*, 34. doi: 10.3389/fncel.2013.00034

Lucchinetti, C. (2011). Taking a Microscopic Look at Multiple Sclerosis. In B. S. Giesser (Ed.), *Primer on Multiple Sclerosis* (pp. 61-77). New York, NY: Oxford University Press.

Lucchinetti, C., Bruck, W., Parisi, J., Scheithauer, B., Rodriguez, M., & Lassmann, H. (2000). Heterogeneity of multiple sclerosis lesions: implications for the pathogenesis of demyelination. *Ann Neurol, 47*(6), 707-717.

Lynch, S. G., Fonseca, T., & LeVine, S. M. (2000). A multiple course trial of desferrioxamine in chronic progressive multiple sclerosis. *Cell Mol Biol (Noisy-le-grand), 46*(4), 865-869.

Mahad, D., Trapp, B. D., & Ransohoff, R. M. (2005). Tissue Pathology of Multiple Sclerosis. In J. Antel, G. Birnbaum, H. P. Hartung & A. Vincent (Eds.), *Clinical Neuroimmunology* (pp. 173-183). New York, NY: Oxford University Press.

Mahad, D., Ziabreva, I., Lassmann, H., & Turnbull, D. (2008). Mitochondrial defects in acute multiple sclerosis lesions. *Brain, 131*(Pt 7), 1722-1735. doi: 10.1093/brain/awn105

Mallory, F. B. (1938). *Pathological Technique*. Philadelphia: W.B. Saunders Co.

Mancall, E. L., & Brock, D. G. (2011). *Gray's Clinical Neuroanatomy: The Anatomic Basis for Clinical Neuroscience*. Philadelphia, PA: Elsevier Saunders.

Martini, F. H., Timmons, M. J., & Tallitsch, R. B. (2015). *Human Anatomy* (8th ed.). Boston, MA: Pearson Education, Inc.

McGill, M. R., & Jaeschke, H. (2013). Oxidant Stress, Antioxidant Defense, and Liver Injury. In N. Kaplowitz & L. D. DeLeve (Eds.), *Drug-Induced Liver Disease* (3rd ed., pp. 71-84). San Diego, USA: Elsevier.

Meguro, R., Asano, Y., Odagiri, S., Li, C., Iwatsuki, H., & Shoumura, K. (2007). Nonheme-iron histochemistry for light and electron microscopy: a historical, theoretical and technical review. *Arch Histol Cytol, 70*(1), 1-19.

Mehta, V., Pei, W., Yang, G., Li, S., Swamy, E., Boster, A., . . . Pitt, D. (2013). Iron is a sensitive biomarker for inflammation in multiple sclerosis lesions. *PLoS One, 8*(3), e57573. doi: 10.1371/journal.pone.0057573

Metz, I., Weigand, S. D., Popescu, B. F., Frischer, J. M., Parisi, J. E., Guo, Y., . . . Lucchinetti, C. F. (2014). Pathologic heterogeneity persists in early active multiple sclerosis lesions. *Ann Neurol, 75*(5), 728-738. doi: 10.1002/ana.24163

Mildner, A., Schmidt, H., Nitsche, M., Merkler, D., Hanisch, U. K., Mack, M., . . . Prinz, M. (2007). Microglia in the adult brain arise from Ly-6ChiCCR2+ monocytes only under defined host conditions. *Nat Neurosci, 10*(12), 1544-1553. doi: 10.1038/nn2015

Miller, L. M., Bourassa, M. W., & Smith, R. J. (2013). FTIR spectroscopic imaging of protein aggregation in living cells. *Biochim Biophys Acta, 1828*(10), 2339-2346. doi: 10.1016/j.bbamem.2013.01.014

Milo, R., & Kahana, E. (2010). Multiple sclerosis: geoepidemiology, genetics and the environment. *Autoimmun Rev, 9*(5), A387-394. doi: 10.1016/j.autrev.2009.11.010

Mirzaei, H., & Regnier, F. (2008). Protein:protein aggregation induced by protein oxidation. *J Chromatogr B Analyt Technol Biomed Life Sci, 873*(1), 8-14. doi: 10.1016/j.jchromb.2008.04.025

Mitrovic, B., Ignarro, L. J., Montestruque, S., Smoll, A., & Merrill, J. E. (1994). Nitric oxide as a potential pathological mechanism in demyelination: its differential effects on primary glial cells in vitro. *Neuroscience, 61*(3), 575-585.

Moll, N. M., Rietsch, A. M., Thomas, S., Ransohoff, A. J., Lee, J. C., Fox, R., . . . Fisher, E. (2011). Multiple sclerosis normal-appearing white matter: pathology-imaging correlations. *Ann Neurol, 70*(5), 764-773. doi: 10.1002/ana.22521

MS International Federation. (2015, October 28, 2015). What is MS? , from https://www.msif.org/about-ms/what-is-ms/

MS Society of Canada. (2016). About MS. Retrieved March 25, 2016, from <https://mssociety.ca/about-ms>

Mukwevho, E., Ferreira, Z., & Ayeleso, A. (2014). Potential Role of Sulfur-Containing Antioxidant Systems in Highly Oxidative Environments. *Molecules, 19*(12), 19376-19389. doi: 10.3390/molecules191219376

Navea, S., Tauler, R., Goormaghtigh, E., & de Juan, A. (2006). Chemometric tools for classification and elucidation of protein secondary structure from infrared and circular dichroism spectroscopic measurements. *Proteins, 63*(3), 527-541. doi: 10.1002/prot.20890

Oberg, K. A., Ruysschaert, J. M., & Goormaghtigh, E. (2004). The optimization of protein secondary structure determination with infrared and circular dichroism spectra. *Eur J Biochem, 271*(14), 2937-2948. doi: 10.1111/j.1432-1033.2004.04220.x

Patrikios, P., Stadelmann, C., Kutzelnigg, A., Rauschka, H., Schmidbauer, M., Laursen, H., . . . Lassmann, H. (2006). Remyelination is extensive in a subset of multiple sclerosis patients. *Brain, 129*(Pt 12), 3165-3172. doi: 10.1093/brain/awl217

Peterson, J. W., Bo, L., Mork, S., Chang, A., & Trapp, B. D. (2001). Transected neurites, apoptotic neurons, and reduced inflammation in cortical multiple sclerosis lesions. *Ann Neurol, 50*(3), 389-400.

Polman, C. H., Reingold, S. C., Banwell, B., Clanet, M., Cohen, J. A., Filippi, M., . . . Wolinsky, J. S. (2011). Diagnostic criteria for multiple sclerosis: 2010 revisions to the McDonald criteria. *Ann Neurol, 69*(2), 292-302. doi: 10.1002/ana.22366

Popescu, B. F., George, M. J., Bergmann, U., Garachtchenko, A. V., Kelly, M. E., McCrea, R. P., . . . Nichol, H. (2009). Mapping metals in Parkinson's and normal brain using rapid-scanning x-ray fluorescence. *Phys Med Biol, 54*(3), 651-663. doi: 10.1088/0031-9155/54/3/012

Popescu, B. F., & Lucchinetti, C. F. (2012a). Meningeal and cortical grey matter pathology in multiple sclerosis. *BMC Neurol, 12*, 11. doi: 10.1186/1471-2377-12-11

Popescu, B. F., & Lucchinetti, C. F. (2012b). Pathology of demyelinating diseases. *Annu Rev Pathol, 7*, 185-217. doi: 10.1146/annurev-pathol-011811-132443

Popescu, B. F., & Nichol, H. (2011). Mapping brain metals to evaluate therapies for neurodegenerative disease. *CNS Neurosci Ther, 17*(4), 256-268. doi: 10.1111/j.1755-5949.2010.00149.x

Popescu, B. F., Pirko, I., & Lucchinetti, C. F. (2013). Pathology of multiple sclerosis: where do we stand? *Continuum (Minneap Minn), 19*(4 Multiple Sclerosis), 901-921. doi: 10.1212/01.CON.0000433291.23091.65

Poser, S., Raun, N. E., & Poser, W. (1982). Age at onset, initial symptomatology and the course of multiple sclerosis. *Acta Neurol Scand, 66*(3), 355-362.

Prinz, M., & Mildner, A. (2011). Microglia in the CNS: immigrants from another world. *Glia, 59*(2), 177-187. doi: 10.1002/glia.21104

Pushie, M. J., Pickering, I. J., Korbas, M., Hackett, M. J., & George, G. N. (2014). Elemental and chemically specific X-ray fluorescence imaging of biological systems. *Chem Rev, 114*(17), 8499-8541. doi: 10.1021/cr4007297

Qi, Y., & Dawson, G. (1994). Hypoxia specifically and reversibly induces the synthesis of ferritin in oligodendrocytes and human oligodendrogliomas. *J Neurochem, 63*(4), 1485-1490.

Quarles, R. H. (2007). Myelin-associated glycoprotein (MAG): past, present and beyond. *J Neurochem, 100*(6), 1431-1448. doi: 10.1111/j.1471-4159.2006.04319.x

Ransohoff, R. M., Hafler, D. A., & Lucchinetti, C. F. (2015). Multiple sclerosis-a quiet revolution. *Nat Rev Neurol, 11*(3), 134-142. doi: 10.1038/nrneurol.2015.14

Ristori, G., Brescianini, S., Pino, A., Visconti, A., Vittori, D., Coarelli, G., . . . Salvetti, M. (2011). Serum elements and oxidative status in clinically isolated syndromes: imbalance and predictivity. *Neurology, 76*(6), 549-555. doi: 10.1212/WNL.0b013e31820af7de

Ropele, S., de Graaf, W., Khalil, M., Wattjes, M. P., Langkammer, C., Rocca, M. A., . . . Fazekas, F. (2011). MRI assessment of iron deposition in multiple sclerosis. *J Magn Reson Imaging, 34*(1), 13-21. doi: 10.1002/jmri.22590

Ross, M. H., & Pawlina, W. (2011). *Histology. A text and atlas.* (6th ed.). Philadelphia, PA: Lippincott Williams and Wilkins.

Rouault, T. A. (2012). Biogenesis of iron-sulfur clusters in mammalian cells: new insights and relevance to human disease. *Dis Model Mech, 5*(2), 155-164. doi: 10.1242/dmm.009019

Schenck, J. (2010). *Pathophysiology of Brain Iron.*

Schrag, M., Dickson, A., Jiffry, A., Kirsch, D., Vinters, H. V., & Kirsch, W. (2010). The effect of formalin fixation on the levels of brain transition metals in archived samples. *Biometals, 23*(6), 1123-1127. doi: 10.1007/s10534-010-9359-4

Slauch, J. M. (2011). How does the oxidative burst of macrophages kill bacteria? Still an open question. *Mol Microbiol, 80*(3), 580-583. doi: 10.1111/j.1365-2958.2011.07612.x

Stephenson, E., Nathoo, N., Mahjoub, Y., Dunn, J. F., & Yong, V. W. (2014). Iron in multiple sclerosis: roles in neurodegeneration and repair. *Nat Rev Neurol, 10*(8), 459-468. doi: 10.1038/nrneurol.2014.118

Storch, M. K., Piddlesden, S., Haltia, M., Iivanainen, M., Morgan, P., & Lassmann, H. (1998). Multiple sclerosis: in situ evidence for antibody- and complement-mediated demyelination. *Ann Neurol, 43*(4), 465-471. doi: 10.1002/ana.410430409

Stuber, C., Morawski, M., Schafer, A., Labadie, C., Wahnert, M., Leuze, C., . . . Turner, R. (2014). Myelin and iron concentration in the human brain: a quantitative study of MRI contrast. *Neuroimage, 93 Pt 1,* 95-106. doi: 10.1016/j.neuroimage.2014.02.026

Suzuki, Y. J., Carini, M., & Butterfield, D. A. (2010). Protein carbonylation. *Antioxid Redox Signal, 12*(3), 323-325. doi: 10.1089/ars.2009.2887

Tegla, C. A., Cudrici, C., Rus, V., Ito, T., Vlaicu, S., Singh, A., & Rus, H. (2009). Neuroprotective effects of the complement terminal pathway during demyelination: implications for oligodendrocyte survival. *J Neuroimmunol, 213*(1-2), 3-11. doi: 10.1016/j.jneuroim.2009.06.006

Thavarajah, R., Mudimbaimannar, V. K., Elizabeth, J., Rao, U. K., & Ranganathan, K. (2012). Chemical and physical basics of routine formaldehyde fixation. *J Oral Maxillofac Pathol, 16*(3), 400-405. doi: 10.4103/0973-029X.102496

Theil, E. C. (1987). Ferritin: structure, gene regulation, and cellular function in animals, plants, and microorganisms. *Annu Rev Biochem, 56,* 289-315. doi: 10.1146/annurev.bi.56.070187.001445

Theil, E. C. (2013). Ferritin: the protein nanocage and iron biomineral in health and in disease. *Inorg Chem, 52*(21), 12223-12233. doi: 10.1021/ic400484n

Thompson, K. J., Fried, M. G., Ye, Z., Boyer, P., & Connor, J. R. (2002). Regulation, mechanisms and proposed function of ferritin translocation to cell nuclei. *J Cell Sci, 115*(Pt 10), 2165-2177.

Todorich, B., Pasquini, J. M., Garcia, C. I., Paez, P. M., & Connor, J. R. (2009). Oligodendrocytes and myelination: the role of iron. *Glia, 57*(5), 467-478. doi: 10.1002/glia.20784

Todorich, B., Zhang, X., & Connor, J. R. (2011). H-ferritin is the major source of iron for oligodendrocytes. *Glia, 59*(6), 927-935. doi: 10.1002/glia.21164

van Horssen, J., Schreibelt, G., Drexhage, J., Hazes, T., Dijkstra, C. D., van der Valk, P., & de Vries, H. E. (2008). Severe oxidative damage in multiple sclerosis lesions coincides with enhanced antioxidant enzyme expression. *Free Radic Biol Med, 45*(12), 1729-1737. doi: 10.1016/j.freeradbiomed.2008.09.023

Vogi, W., Nolte, R., & Brunahl, D. (1991). Binding of iron to the 5th component of human complement directs oxygen radical-mediated conversion to specific sites and causes nonenzymic activation. *Complement Inflamm, 8*(5-6), 313-319.

Webb, S., & Roach, C. (2014). *SSRL School on Synchrotron X-ray Microscale Imaging Techniques*. Powerpoint slides. SLAC National Accelerator Laboratory.

Wegner, C., Esiri, M. M., Chance, S. A., Palace, J., & Matthews, P. M. (2006). Neocortical neuronal, synaptic, and glial loss in multiple sclerosis. *Neurology, 67*(6), 960-967. doi: 10.1212/01.wnl.0000237551.26858.39

Weigel, K. J., Lynch, S. G., & LeVine, S. M. (2014). Iron chelation and multiple sclerosis. *ASN Neuro, 6*(1), e00136. doi: 10.1042/AN20130037

Witte, M. E., Mahad, D. J., Lassmann, H., & van Horssen, J. (2014). Mitochondrial dysfunction contributes to neurodegeneration in multiple sclerosis. *Trends Mol Med, 20*(3), 179-187. doi: 10.1016/j.molmed.2013.11.007

Yamamoto, T., & Hirano, A. (1986). A comparative study of modified Bielschowsky, Bodian and thioflavin S stains on Alzheimer's neurofibrillary tangles. *Neuropathol Appl Neurobiol, 12*(1), 3-9.

Yao, B., Ikonomidou, V. N., Cantor, F. K., Ohayon, J. M., Duyn, J., & Bagnato, F. (2015). Heterogeneity of Multiple Sclerosis White Matter Lesions Detected With T2*-Weighted Imaging at 7.0 Tesla. *J Neuroimaging, 25*(5), 799-806. doi: 10.1111/jon.12193

Ye, H., & Rouault, T. A. (2010). Human iron-sulfur cluster assembly, cellular iron homeostasis, and disease. *Biochemistry, 49*(24), 4945-4956. doi: 10.1021/bi1004798

Zecca, L., Youdim, M. B., Riederer, P., Connor, J. R., & Crichton, R. R. (2004). Iron, brain ageing and neurodegenerative disorders. *Nat Rev Neurosci, 5*(11), 863-873. doi: 10.1038/nrn1537

Zhang, X., Haaf, M., Todorich, B., Grosstephan, E., Schieremberg, H., Surguladze, N., & Connor, J. R. (2005). Cytokine toxicity to oligodendrocyte precursors is mediated by iron. *Glia, 52*(3), 199-208. doi: 10.1002/glia.20235

Zheng, W., Nichol, H., Liu, S., Cheng, Y. C., & Haacke, E. M. (2013). Measuring iron in the brain using quantitative susceptibility mapping and X-ray fluorescence imaging. *Neuroimage, 78*, 68-74. doi: 10.1016/j.neuroimage.2013.04.022

Zhong, Y., Utriainen, D., Wang, Y., Kang, Y., & Haacke, E. M. (2014). Automated White Matter Hyperintensity Detection in Multiple Sclerosis Using 3D T2 FLAIR. *Int J Biomed Imaging, 2014*, 239123. doi: 10.1155/2014/239123